The Decoherence of Spin Chains Coupled to an Electron Bath

Bachelor Thesis

by

Marit Piek

to obtain the degree of Bachelor of Science
at the Delft University of Technology,
to be defended publicly on Tuesday June 27, 2023 at 10:00 AM.

Student number:	5157552	
Project duration:	November 14, 2022 – June 27, 2023	
Thesis committee:	Prof. Dr. A.F. Otte,	TU Delft, supervisor
	Prof. Dr. P.M. Visser,	TU Delft, supervisor
	R. Broekhoven,	TU Delft, supervisor
	Prof. Dr. J. M. Thijssen,	TU Delft
	Dr. B. Janssens,	TU Delft

An electronic version of this thesis is available at `http://repository.tudelft.nl/`.

Abstract

Recent advancements in research technology have enabled the analysis of matter at the atomic level, allowing for the investigation of peculiar quantum mechanical phenomena, such as the time evolution of coherent quantum states [8]. This thesis takes the initial steps towards modelling the decoherence of magnetic atoms on a conducting surface, considering the coupling between the atoms and the surface leading to the decoherence of the spin state in a chain of atoms.

To characterise the relaxation and decoherence of a spin chain, the Lindblad equation is employed to describe the Kondo interaction with the surface. Two models are presented: one that considers interactions at the level of individual atoms, and another that incorporates the impact of the environment on the collective state of the chain. These models provide insight into the dynamic behaviour and decoherence of various adatom chain configurations. The analysis reveals a steady decrease in coherence time with an increasing chain length. Furthermore, it is demonstrated that the decay rate scales linearly with temperature for a chain of two atoms.

In addition, this thesis explores the scenario of asymmetric coupling, where only one atom is coupled to the surface. The results show that, for a two-atom chain, the coherence time is doubled in the asymmetric case. However, conclusive findings could not be drawn for longer chains. These results hold promise for future research and improvement of the model.

Contents

Chapter 1

Introduction

Quantum information processing has emerged as a promising field with the potential to revolutionise computing, communication, and cryptography. Central to the development of quantum technologies is the requisite to effectively control and manipulate quantum states. However, quantum systems are fragile and susceptible to decoherence [5], which refers to the loss of coherence and entanglement due to unwanted interactions with the surrounding environment. Understanding and mitigating decoherence effects are fundamental challenges in the realisation of practical quantum devices.

In recent years, one-dimensional spin chains have attracted considerable attention as potential candidates for quantum information processing [15]. These spin chains serve as excellent platforms for studying the intricate interplay between quantum coherence and environmental interactions. A crucial aspect in this context is the coupling of the spin chain to an electron bath, which can significantly affect the coherence properties of the system [5]. In figure 1.1 a one-dimensional spin chain coupled to an electron bath is depicted.

The primary objective of this thesis is to investigate the decoherence and dynamics of magnetic adatoms which form a spin chain coupled to an electron bath. By employing the Lindblad equation as the theoretical framework for our analysis, our aim is to unravel the dynamics of the system and the scaling of the decoherence with respect to the chain length and it's interaction with the bath.

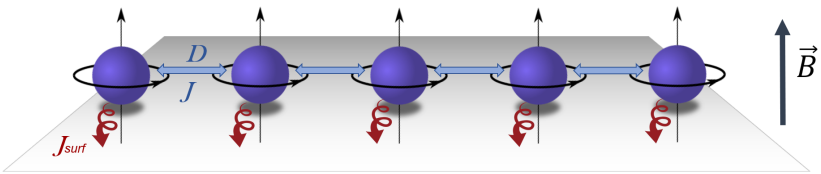

Figure 1.1: One dimensional spin chain of five atoms coupled by a surface coupling J_{surf} (red arrow) to an electron bath. The atoms experience a coupling with one another (blue arrow) in the form of exchange coupling J, and dipolar coupling D. The magnetic adatoms are in an external magnetic field $\vec{B}$, and the black arrows pointing upwards represent their respective spin states.

The models constructed using the Lindblad equation are intended to enhance and support experimental observations, including those obtained through techniques such as scanning tunnelling microscopy (STM). An STM uses a fine needle-shaped probe to scan the surface of a material. When a voltage is applied between the probe and the material, a tunnelling current flows, which is highly sensitive to the distance between the probe and the surface. This current is measured and used to create a topographic map of the material's surface with exceptional resolution, even down to the atomic level. For studying magnetisation of atoms, the most well-known is spin-polarised STM (SP-STM), where different magnetisation orientations of the spins result in different conductance values [13]. Using STM, various configurations of magnetic adatoms can be created by bringing the tip close to weakly coupled atoms and dragging them across the surface. Figure 1.2 shows the construction of a chain of atoms enabled by an STM.

A significant discovery has recently emerged, sparking rapid advancements in this field. Baumann et al. [1]

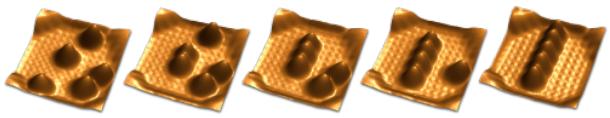

Figure 1.2: STM images showing the construction of a chain of atoms (each approximately 5 nm wide). *Source: Ottelab* [12]

.

revealed that the STM can now be modified to perform electron spin resonance, allowing for both high spatial resolution and high energy resolution simultaneously. Additionally, the ESR enables coherent spin manipulation. In ESR-STM (electron spin resonance-STM), a radio frequency signal is sent down the STM tip. This causes the atom beneath the tip to respond with a Rabi rotation, resulting in a change in the spin-polarised conductance only when the drive signal is in resonance with the procession of the spin [1]. This technique gives very precise information in terms of energy transitions. Additionally, advanced techniques can be employed, like ultrafast pump-probe spectroscopy, for snapshot measurements of the system's time evolution on the nanosecond timescale. The pump-probe technique involves the interaction of two laser pulses: a "pump" pulse and a "probe" pulse. The pump pulse initiates an excitation or perturbation in the quantum system, while the probe pulse measures the system's response after a certain time delay [8].

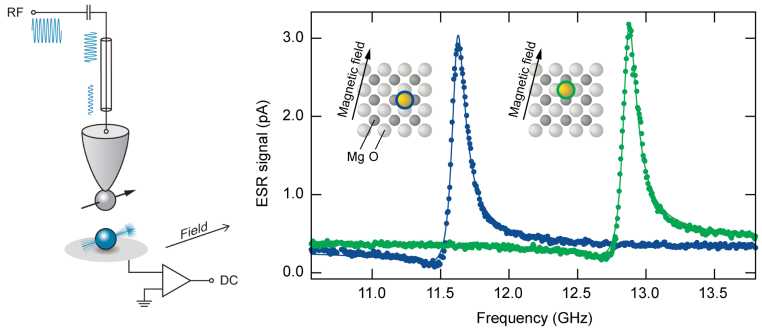

Figure 1.3: ESR measurement of a Ti atom on an MgO lattice structure, in two different spatial orientations with respect to the magnetic field. On the left a radio frequency signal is sent down the STM tip, resulting in a Rabi rotation of the atom. On the right it can be seen that the two spatial orientations of the Ti atom result in a different energy peak. This illustrates the tremendous resolution in terms of energy provided by ESR-STM. *Source: Veldman et al. [15]*

.

A suitable spin-$\frac{1}{2}$ system that will be considered consists of Ti-adatoms on a bilayer MgO substrate atop an Ag[100] crystal [15]. Here Kondo interaction plays the most significant role in spin decoherence [5]. The relaxation (T_1) and decoherence (T_2) time scale with the coupling strength of the Ti atom to the surface. This coupling strength is relatively weak due to the insulating bilayer of MgO [15]. Two models based on the Lindblad equation will be explored: one considering interactions on individual atoms and the other incorporating the effect of the environment on the chain's energy eigenstates. These models will allow us to predict the dynamic behaviour and decoherence of any adatom chain configuration.

The thesis is organised as follows: it begins by providing the necessary theoretical foundations to describe our quantum system (Ch. 2). Then, the system Hamiltonian is introduced that governs our adatom spin chain (Ch. 3). In Chapter 4, the aforementioned models based on the Lindblad equation will be derived. Subsequently, an analytical solution of the model is presented (Ch. 5) to serve as a reference for verifying our numerical implementation, the results of which will be discussed in chapter 6. Finally, conclusions are drawn and avenues for further research are suggested in the concluding chapter (Ch. 7).

Chapter 2

Theory

This chapter introduces the mathematical formalism used to describe spin operators and spin states. Subsequently, the construction of the Hamiltonian and the derivation of the equations governing the time evolution of the system are discussed. Finally, decoherence and it's primary cause in our system, namely the Kondo interaction, are introduced.

2.1. Operators

Observables in quantum mechanics, such as position, momentum, energy, and spin, are associated with specific operators. These operators have eigenvalues and corresponding eigenvectors that represent the possible measurement outcomes and the corresponding states of the system. This section establishes the formalism and definitions concerning operators and states that will be employed throughout this thesis.

2.1.1. Spin Operators

The Pauli matrices span the space of observables of the complex 2-dimensional Hilbert space. They represent the component of the spin in the $\hat{x}$, $\hat{y}$, and $\hat{z}$-direction [11].

$$\hat{\sigma}_x = \begin{pmatrix} 0 & 1 \\ 1 & 0 \end{pmatrix} \tag{2.1}$$

$$\hat{\sigma}_y = \begin{pmatrix} 0 & -i \\ i & 0 \end{pmatrix} \tag{2.2}$$

$$\hat{\sigma}_z = \begin{pmatrix} 1 & 0 \\ 0 & -1 \end{pmatrix} \tag{2.3}$$

Using the Pauli matrices the Spin operators for spin-$\frac{1}{2}$ particles are defined:

$$\hat{S}_x = \frac{\hbar}{2}\hat{\sigma}_x, \quad \hat{S}_y = \frac{\hbar}{2}\hat{\sigma}_y, \quad \hat{S}_z = \frac{\hbar}{2}\hat{\sigma}_z. \tag{2.4}$$

For convention the eigenvectors of $\hat{S}_z$ are chosen as basis. The factor $\hbar$ is left out for simplicity. The eigenstates of $\hat{S}_z$ are our basis vectors: [11]:

$$|0\rangle = |\downarrow\rangle = \begin{pmatrix} 1 \\ 0 \end{pmatrix}, \text{ and } |1\rangle = |\uparrow\rangle = \begin{pmatrix} 0 \\ 1 \end{pmatrix}. \tag{2.5}$$

The raising and lowering operator, also known as ladder operators are:

$$\hat{S}_\pm = \frac{1}{2}(\hat{S}_x \mp i\hat{S}_y). \tag{2.6}$$

2.1.2. Tensor Product

When working with multiple particles, in order to describe the system, a product space needs to be defined using the tensor product. The tensor product of two vector spaces V and W is denoted as: $V \otimes W$. The operation $\otimes$ sends ordered pairs of the Cartesian product $V \times W$ to $V \otimes W$.

Basis states of a two spin-$\frac{1}{2}$ particle system
The basis states of a two spin-$\frac{1}{2}$ particle system are (ranging from lowest to highest eigenvalue):

$$|\downarrow\downarrow\rangle = |\downarrow\rangle \otimes |\downarrow\rangle = \begin{pmatrix} 1 \\ 0 \\ 0 \\ 0 \end{pmatrix}, \quad |\downarrow\uparrow\rangle = |\downarrow\rangle \otimes |\uparrow\rangle = \begin{pmatrix} 0 \\ 1 \\ 0 \\ 0 \end{pmatrix}, \quad |\uparrow\downarrow\rangle = |\uparrow\rangle \otimes |\downarrow\rangle = \begin{pmatrix} 0 \\ 0 \\ 1 \\ 0 \end{pmatrix}, \quad |\uparrow\uparrow\rangle = |\uparrow\rangle \otimes |\uparrow\rangle = \begin{pmatrix} 0 \\ 0 \\ 0 \\ 1 \end{pmatrix}. \tag{2.7}$$

Using the tensor product, these basis states can be extended to the basis states of an N-particle system.

Extending operators to N-particle systems
In order to work with N-particle systems, the operators need to be expanded so that they act on the larger Hilbert space. Taking an initial operator $\hat{T}$, the aim is to describe the operator acting solely on the k^{th} particle. This is achieved by taking the tensor product of N matrices of which the k^{th} matrix is the operator $\hat{T}$ and the other matrices are identity matrices of the same dimensions:

$$\hat{T}(k) = I \otimes I \otimes ... \otimes \hat{T} \otimes ... \otimes I. \tag{2.8}$$

The corresponding operator for the whole system is the sum of the individual operators [11]:

$$\hat{T}_N = \sum_{k=1}^{N} \hat{T}(k). \tag{2.9}$$

2.2. System Hamiltonian

The Hamiltonian $\hat{H}$ of a system consisting of N spin-$\frac{1}{2}$ particles, where the the exchange coupling J, the dipolar coupling D, and a global magnetic field $\mathbf{B}$ are considered, is given by:

$$\hat{H} = \sum_{i}^{N-1} \left((J+2D)\hat{S}_z^{(i)}\hat{S}_z^{(i+1)} + (J-D)(\hat{S}_x^{(i)}\hat{S}_x^{(i+1)} + \hat{S}_y^{(i)}\hat{S}_y^{(i+1)}) \right) + \sum_{i}^{N} \left(g\mu_B \mathbf{B} \cdot \hat{\mathbf{S}}^{(i)} \right). \tag{2.10}$$

In this expression S is the spin magnitude, g the g-factor, and μ_B the Bohr magneton.

2.2.1. Zeeman Interaction

The Zeeman effect arises from the interaction between the magnetic moment of a particle or system and an external magnetic field. Spin-$\frac{1}{2}$ particles have magnetic moment along the direction of their spin [14]. The interaction between the magnetic moment and the field leads to the splitting of energy levels. The energy levels with parallel alignment experience a lower energy, while the energy levels with antiparallel alignment have a higher energy. The energy difference between these levels is proportional to the strength of the external magnetic field. To incorporate the Zeeman effect into the Hamiltonian, a term of the form:

$$\hat{H}_{\text{Zeeman}} = \sum_{i}^{N} \left(g\mu_B \mathbf{B} \cdot \hat{\mathbf{S}}^{(i)} \right) \tag{2.11}$$

is introduced. Here, N represents the number of particles in the system, g is the gyromagnetic ratio, μ_B is the Bohr magneton, $\mathbf{B}$ is the external magnetic field vector, and $\hat{\mathbf{S}}^{(i)}$ represents the spin operator of the i-th particle. This term captures the interaction energy between the magnetic moment of each particle and the external magnetic field. The dot product between the magnetic field and the spin operator accounts for the alignment or anti-alignment of the spin with respect to the field, determining the splitting and shifts in energy levels.

2.2.2. Dipolar Interaction

In addition to the interaction with the external magnetic field, the spins also interact with each other via dipolar interaction. Following the classical description of the dipole-dipole interaction, the corresponding term in the Hamiltonian is defined as [16]:

$$\hat{H}_{\text{Dipolar}} = D_0 \sum_{i}^{N-1} \left[\hat{\mathbf{S}}^{(i)} \cdot \hat{\mathbf{S}}^{(i+1)} - 3(\hat{\mathbf{S}}^{(i)} \cdot \hat{n})(\hat{\mathbf{S}}^{(i+1)} \cdot \hat{n}) \right]. \tag{2.12}$$

Here $\hat{n}$ is the inter-atomic unit vector, and D_0 is the dipolar constant. The dipolar constant decreases rapidly with inter-atomic distance r:

$$D_0 = \frac{\mu_0 \gamma_1 \gamma_2 \hbar^2}{4\pi r^3},$$

where μ_0 is the permeability of vacuum, and γ_i are the gyromagnetic ratios of the corresponding atoms. This rapid decrease with r explains why only nearest-neighbour dipolar interaction is considered. Furthermore, for high magnetic fields the secular approximation can be used which amounts to neglecting the coupling terms between states of different energies [4]. In the presence of a high magnetic field, the energy differences between states become significant, causing rapid oscillations in coherences. The secular approximation takes advantage of this rapid oscillation to neglect terms that average out to zero over time. By employing the secular approximation, the dipolar interaction Hamiltonian can be simplified to a Heisenberg-like spin Hamiltonian with distinct prefactors for the $z-z$ interaction and the $x-x$, $y-y$ interactions [4]:

$$\hat{H}_{\text{Dipolar}} = D \sum_{i}^{N-1} \left[2\hat{S}_z^{(i)} \hat{S}_z^{(i+1)} - \hat{S}_x^{(i)} \hat{S}_x^{(i+1)} - \hat{S}_y^{(i)} \hat{S}_y^{(i+1)} \right]. \tag{2.13}$$

It is important to note that the secular approximation is valid when the energy differences between different terms in the dipolar interaction are much larger than the characteristic frequencies of the system. In eq. 2.13, D is the dipolar coupling constant. The relation between the dipolar coupling of two atoms subject to an in plane magnetic field (B_z in the $[1,1,0]-$ direction) and the interatomic distance r is [16] [2]:

$$D = \frac{\mu_0 \mu_i^2 (1 - 3\cos^2\theta)}{2\pi r^3} = \frac{1}{2} D_0 (1 - 3\cos^2\theta), \tag{2.14}$$

where θ is the angle between the connecting vector $\hat{r}$ and the direction of the applied magnetic field, μ_i is the magnetic moment of the atom, and μ_0 is the permeability of vacuum.

2.2.3. Exchange Interaction

Another important interaction between the atoms is the exchange interaction. This is a quantum mechanical effect that occurs between identical particles. When the wavefunctions of indistinguishable particles overlap, they are subject to exchange symmetry. For fermions, this results in the increase of the expectation value of the distance, and is therefore sometimes referred to as Pauli repulsion. Since by the Pauli exclusion principle two fermions cannot occupy the same state, the overall quantum state is required to be antisymmetric. As a result, electrons are so to speak "exchanged" between atoms. If this happens directly the effect is known as covalent bonding; if it is mediated through a non-magnetic atom it is known as superexchange. Both interactions are isotropic and decay exponentially with the distance between particles. Therefore, only nearest-neighbour exchange interaction is considered, allowing for it to be modelled by a Heisenberg spin Hamiltonian:

$$\hat{H}_{\text{Exchange}} = J \sum_{i}^{N-1} \hat{\mathbf{S}}^{(i)} \cdot \hat{\mathbf{S}}^{(i+1)}. \tag{2.15}$$

In this equation J is the coupling strength.

Combining the equations for the Zeeman interaction (Eq. 2.11), the dipolar interaction (Eq. 2.13), and the exchange interaction (Eq. 2.15), to obtain the the system Hamiltonian that was previously stated in Eq. 2.10.

2.3. Density Matrix

Density matrices are powerful tools for representing quantum states, particularly in cases where the state is mixed and cannot be fully described by a wave function or a pure state vector. In such scenarios, the density matrix provides the optimal specification of the system. It is defined as:

$$\hat{\rho} = \sum_i p_i \left|\phi_i\right\rangle \left\langle\phi_i\right|. \tag{2.16}$$

Here p_i represents the probability of finding the system in the state $|\phi_i\rangle$. The states $|\phi_i\rangle$ form a complete and orthonormal set, and the sum of the probabilities should equal one, i.e. $\sum_i p_i = 1$.

In any basis, the diagonal entries are known as occupations, and represent the probabilities to finding the system in each of its basis states. Shifts in occupations are called relaxations (decrease of total energy) or excititations (increase of total energy). The off-diagonal entries are the coherences, which represent the possibility

of finding a system in a superposition of basis states. The density matrix is useful for calculating the expectation value of an operator. The expected value of an operator a certain in state (eq. 2.16) is given by;

$$\langle \hat{T} \rangle = tr(\hat{\rho}\hat{T}) = \sum_i^n p_i \mathrm{Tr}(|\phi_i\rangle \langle \phi_i| \hat{T}) = \sum_i^n p_i \langle \phi_i| \hat{T} |\phi_i\rangle . \tag{2.17}$$

In this equation, $\mathrm{Tr}(\hat{\rho}\hat{T})$ denotes the trace, meaning the sum of the diagonal elements. Consequently, observe that $\langle \hat{T} \rangle$ is the average of the expectation values for the pure states $|\phi_i\rangle$.

2.4. Time Evolution

The time dependent state of a quantum system is of interest. The Schrödinger equation describes the time-evolution of the wave function:

$$\frac{\mathrm{d}}{\mathrm{d}t} |\phi(t)\rangle = -\frac{i}{\hbar} \hat{H} |\phi(t)\rangle . \tag{2.18}$$

The Von Neumann equation is equivalent to the Schrödinger equation, except it describes the time evolution of the density matrix:

$$\frac{\mathrm{d}\hat{\rho}}{\mathrm{d}t} = -\frac{i}{\hbar} [\hat{H}, \hat{\rho}]. \tag{2.19}$$

2.5. Decoherence

In quantum mechanics, particles can exist in a superposition of states, where they can be in multiple states simultaneously. As long as there is a definite phase relation between the different states, the system is said to be coherent. If a quantum system would be perfectly isolated, it would remain coherent. However, due to entanglement with the environment, the system will dissipate information and therefore lose it's coherence. This decay of coherence is called decoherence, and it has a characteristic decoherence rate. For a two level system, the total system decoherence time is denoted T_2.

Relaxation, also known as dissipation, is a specific type of decoherence process that involves the loss of energy or population from a quantum system. In relaxation, the system tends to approach a state of thermal equilibrium with its surroundings. This process occurs when a system interacts with a heat bath or a reservoir and exchanges energy, causing the system to transition to lower or higher energy states (depending on the temperature of the heat bath). Relaxation leads to the decay of excited states and the thermalisation of the system. It is associated with the relaxation time or characteristic time scale over which the system returns to equilibrium. For a two level system, the characteristic time of evolution towards the equilibrium state is T_1.

Pure dephasing is another type of decoherence process that affects the coherence of a quantum system. In pure dephasing, the loss of coherence occurs without any loss of energy or population. It is specifically associated with the loss of phase coherence in a superposition state. Pure dephasing arises from interactions between the system and its environment, which introduce random fluctuations in the phase of the quantum state. These fluctuations cause the different components of the superposition to accumulate different phase factors, resulting in the loss of interference effects. Pure dephasing is often characterised by a dephasing time, which represents the timescale over which the phase coherence is lost. For a two level system, the characteristic time of pure dephasing is T_ϕ.

As can be derived through for example Bloch Redfield T_1, T_2 and T_ϕ are related as follows [5]:

$$\frac{1}{T_2} = \frac{1}{2T_1} + \frac{1}{T_\phi}. \tag{2.20}$$

2.5.1. Kondo Interaction

The Kondo interaction has been found to be the most prominent interaction between magnetic adatoms and the surface [17]. It arises from the interaction between s-wave electrons of the conducting surface and d-shell electrons in the adatoms. This interaction can be modelled as Heisenberg point-point contact interactions between the spins, as it originates from the exchange interaction and diminishes with distance. Notably, at

low temperatures, the interaction is centred around the Fermi wave number, allowing for an approximate independence from the wave number. For magnetic adatoms on a surface the Kondo exchange interaction Hamiltonian is [5] [2]:

$$\hat{H}_{\text{Kondo}} = \sum_{n,a} J_n S_a^{(n)} \otimes s_a^{(n)}. \tag{2.21}$$

In this equation, n is the sum over the adatoms, and $a = \{x, y, z\}$. $S_a^{(n)}$ is the n^{th} adatom spin projection in the a-direction, $s_a^{(n)}$ the surface spin projection density at the position of adatom n, and J the spin-spin Heisenberg interaction strength.

In the study by Loth et al. [9], the interaction between the adatom's and surface electrons is incorporated into the Pauli rates. The conventional model for inelastic electron tunnelling is employed to describe the transition rate from the system's eigenstate $|i\rangle$ to $|j\rangle$ [7] [2]:

$$\begin{aligned} r_{i\to j} &= \frac{G_S}{e^2} P_{i\to j} \int_{-\infty}^{+\infty} f(E)\left[1 - f\left(E - E_j + E_i\right)\right] dE \\ &= \frac{G_S}{e^2} P_{i\to j} \frac{\epsilon_{ij}}{e^{\frac{\epsilon_{ij}}{k_B T}} - 1}, && \text{if } E_i \neq E_j, \\ &= \frac{G_S}{e^2} P_{i\to j} k_B T, && \text{if } E_i = E_j. \end{aligned} \tag{2.22}$$

Here, f represents the Fermi function $f(E) = \left(1 + e^{-\frac{\epsilon_{ij}}{k_B T}}\right)^{-1}$. E_i and E_j are the eigenenergies of the initial and final states, respectively, and ϵ_{ij} denotes their energy difference. The prefactor G_s (the surface-atom-surface conductance) characterises the strength of the spontaneous relaxation and is governed by conduction through the thin insulating layer of MgO. The transmission coefficients $P_{i\to j}$ relate the probability of spin scattering through Kondo interaction per unit time to the quantum mechanical transition intensities:

$$P_{i\to j} = \frac{1}{P_0} \sum_{\sigma_k, \sigma_{k'}} |\langle i\sigma_k | \hat{\sigma} \cdot \hat{\mathbf{S}} | j\sigma_{k'} \rangle|^2. \tag{2.23}$$

In the above equation, σ_k and $\sigma_{k'}$ represent the initial and final spin states of the scattering electron, respectively. Thus, $|i\sigma_k\rangle$ corresponds to the product state of the atom's spin and the scattering electron spin. P_0 is a normalisation factor. This transition intensity is based on the exchange interaction between the scattering electron and the adatom's spin [9]. Transitions within the same eigenstate $|i\rangle$ (i.e., $i = j$) are considered to account for pure dephasing.

2.6. The Lindblad Equation

In order to model coupling of a quantum system to its environment, an approximation is needed of the decoherence of this quantum system. If L_k is any jump operator (multiplied by the correct weighing factor) that describes the decoherence is acting on the particle k (e.g. the spin lowering operator, eq. 2.6), the Liouvillian is given by [10]:

$$\hat{L_k}\hat{\rho}\hat{L}_k^\dagger - \frac{1}{2}\hat{L}_k^\dagger \hat{L}_k \hat{\rho} - \frac{1}{2}\hat{\rho}\hat{L}_k^\dagger \hat{L}_k. \tag{2.24}$$

Then, under strong approximations, the Lindblad equation is obtained from the Von Neumann equation by adding the Liouvillian, and summing over all particles [10]:

$$\frac{\mathrm{d}\hat{\rho}}{\mathrm{d}t} = -\frac{i}{\hbar}[\hat{H}, \hat{\rho}] + \sum_k \hat{L_k}\hat{\rho}\hat{L}_k^\dagger - \frac{1}{2}\sum_k \{\hat{L}_k^\dagger \hat{L}_k, \hat{\rho}\}. \tag{2.25}$$

The transformation from the Von Neumann equation to the Lindblad equation involves a series of approximations:

- **Second-order perturbation theory**
  Assuming a weak coupling between the system and its environment, the interaction with the environment can be estimated as as a second order perturbation on the unperturbed system evolution. For

the system of Ti-atoms that under consideration this assumption is justified by the insulating bilayer of MgO.

- **Markov approximation**
  The Markov approximation assumes that the environment acts as a Markovian bath and that the memory effects of the environment are negligible. It implies that the system's dynamics only depend on its instantaneous state and not its past history. It is valid when the environment correlation time is much smaller than the system's time scale. This assumption is plausible for the relatively large MgO surface that is involved.

- **Born approximation**
  The Born approximation assumes that because of the weak coupling to a large environment, the environment state hardly differs from the uncoupled thermal equilibrium state. In this way, the spin chain state and the environment state are always separable; and the environment is always in thermal equilibrium.

- **Strong secular approximation**
  As previously mentioned in section 2.2.2, terms that oscillate rapidly average out to zero over time, and can therefore be neglected. In the case of a slower system evolution, these are approximately only the constant terms. As a result of considering only these terms, there is no coupling between coherences and occupations. This is only valid for weak interactions [3].

Furthermore, since the perturbed Von Neumann equation is usually solved via time integration, the requisite for the integration step must be that the collective spin state of the chain does not evolve in it. Meaning the system evolution time must be much larger than the integration time step.

2.7. Thermal Equilibrium

If there is no symmetry that prevents the change of occupations, the Boltzmann thermal equilibrium equation provides a description of the occupation probabilities of energy levels in a system. The occupation of energy level E_i is as follows: $p_i = \frac{e^{-E_i/k_BT}}{Z}$, where k_B is the Boltzmann constant, T the temperature, and $Z = \sum_i e^{-E_i/k_BT}$ the normalisation factor. Therefore, the density matrix of the equilibrium state is given by [5]:

$$\begin{aligned} \rho(t \to \infty) = \overline{\rho} &= \sum_i |E_i\rangle \langle E_i| \frac{e^{-E_i/k_BT}}{Z} \\ &= \frac{e^{-H/k_BT}}{Z}. \end{aligned} \tag{2.26}$$

where the summation is over the possible energy states i. Notice that the second part of the expression is justified since $H|E_i\rangle = E_i|E_i\rangle$.

2.7.1. High and Low Temperature Limits

At low temperatures, when T is small, the exponential term e^{-E_i/k_BT} becomes significant for energy levels with lower values of E_i. Since the exponential term decreases rapidly with decreasing E_i, the probability p_i is highest for the energy levels with the lowest values. In other words, the lower energy levels are the preferred occupation. This behaviour is commonly observed in systems at low temperatures and is known as the Bose-Einstein condensation (in the case of bosons) or Fermi-Dirac distribution (in the case of fermions).

However, as the temperature increases, the exponential term e^{-E_i/k_BT} becomes less significant, and the occupation probabilities are no longer strongly dependent on the energy levels. In the high-temperature limit, when T is large, the exponential term tends to approach unity ($e^{-E_i/k_BT} \to 1$) for all energy levels E_i. Consequently, the occupation probabilities p_i become approximately equal for all energy levels. The reason behind this behaviour lies in the relative magnitudes of thermal energy (k_BT) and the energy differences between the levels. At high temperatures, the thermal energy is comparable to or larger than the energy spacing between different energy levels. As a result, the system has sufficient energy to access a wide range of energy levels, and the probabilities of occupation become more evenly distributed.

Chapter 3

System Hamiltonian for Multiple Atoms

The goal of this chapter is to understand the dynamic behaviour of spin particle chains. The first section explains how the Hamiltonian is constructed, including the influence of a global magnetic field on the eigenstates. In the second section, the time-evolution governed by the Hamiltonian is studied.

3.1. Construction of the Time-Independent Hamiltonian

Recall the Hamiltonian given previously by equation 2.10:

$$\hat{H} = \sum_{i}^{N-1} \left((J+2D)\hat{S}_z^{(i)} \hat{S}_z^{(i+1)} + (J-D)(\hat{S}_x^{(i)} \hat{S}_x^{(i+1)} + \hat{S}_y^{(i)} \hat{S}_y^{(i+1)}) \right) + \sum_{i}^{N} \left(g\mu_B \mathbf{B} \cdot \hat{\mathbf{S}}^{(i)} \right). \tag{3.1}$$

To explain how the multi-particle operators act on the Hilbert space, each term starts with a tensor product $\prod_{n=1}^{N} \mathbb{1}(S_n)$, where $\mathbb{1}(S_n)$ are the identity matrices of dimension $(2S_n+1)$. After that, the i^{th} identity matrix is replaced with a spin operator to find the operator working on the i^{th} particle. All the terms are added together to get our final expression for the Hamiltonian. Using the package *QuTip* the systems eigenstates and corresponding eigenenergies can easily be calculated [6] . Figure 3.1 depicts the Zeeman splitting of a three spin-$\frac{1}{2}$ particle system where the global magnetic field has a magnitude of 10 mT in the z-direction (and the dipolar and exchange coupling were set to zero, and $g = 1.98$).

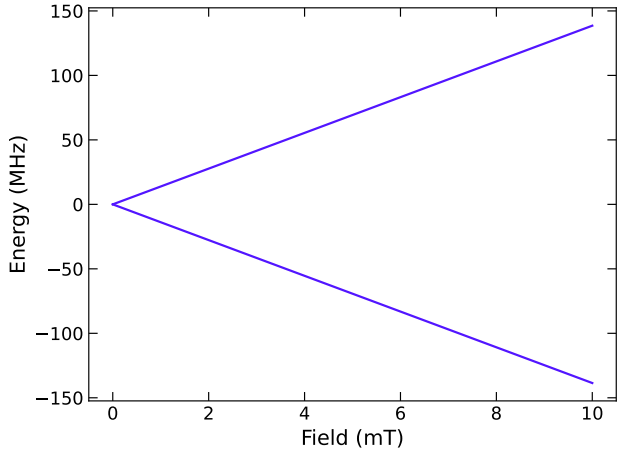

Figure 3.1: Zeeman splitting: The eigenenergies of a spin-$\frac{1}{2}$ particle vs the global magnetic field. For a field along the z-axis, the eigenstates are $|\uparrow\rangle$ and $|\downarrow\rangle$

.

3.2. Evolution of the Time-Dependent Hamiltonian

Consider a spin-$\frac{1}{2}$ particle in a magnetic field of 100 mT in the z-direction. Our system is prepared in the spin up state and the corresponding density matrix is defined according to equation 2.16. Then the Von Neumann equation eq. 2.19 is solved using the *QuTip* function sesolve [6]. In figure 3.2 the time evolution of the spin expectation value can be seen, with Larmor precession in the x and y directions.

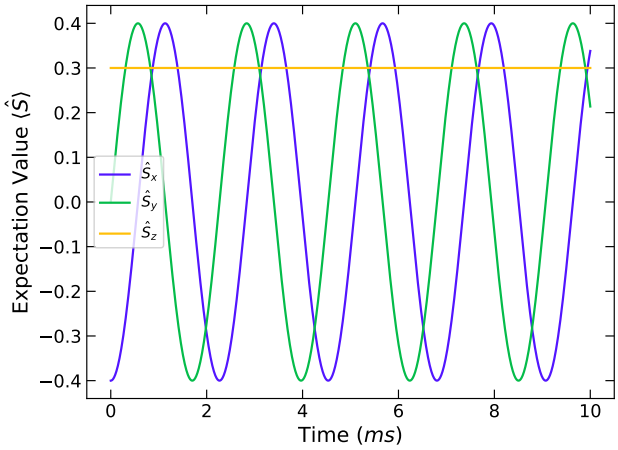

Figure 3.2: Time evolution of the expectation value of the three components of the spin vector of a spin-$\frac{1}{2}$ particle in a magnetic field of 100 mT, initially in spin up. The z-component is constant.

3.3. Modelling Ti-atoms on a Surface

It has been found using ESR measurement and tunnel spectroscopy that Ti adatoms on a bilayer of MgO subject to an in plane magnetic field often have an effective spin $\frac{1}{2}$ [16]. In order to model a chain of Ti-atoms, realistic values for the exchange coupling strength J, the dipolar coupling strength D, and the g-factor g are needed.

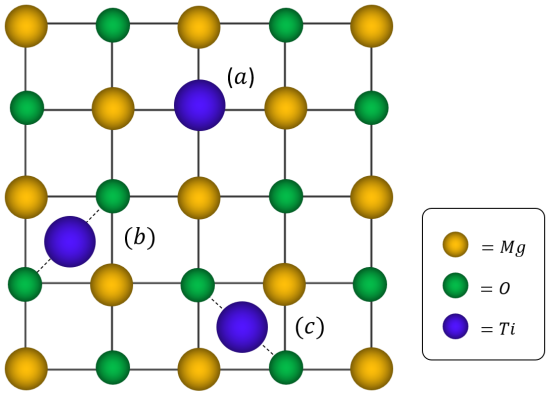

Figure 3.3: Schematic of a MgO lattice with Ti adatoms. (a) Oxygen bound Ti, (b) Ti bound to bridge site of two oxygen atoms, (c) different spatial orientation of Ti atom bound to a bridge site

The Ti-atoms can either be bound to an oxygen atom or on the bridge site between two oxygen atoms as is depicted in figure 3.3, and as a result they have different gyromagnetic ratios [15]. For the dipolar coupling strength D, as given by eq. 2.14, the value of $D_0 = 78 \pm 17$ MHz at r_0 (three lattice constants, $r_0 = 8.64$ Å) [16].

The following relation for exchange coupling strength of oxygen bound Ti atoms J with respect to interatomic distance r has been found [16]:

$$J = J_0 e^{\frac{-(r-r_0)}{d_{ex}}} \tag{3.2}$$

Where the decay constant was found to be $d_{ex} = 0.40 \pm 0.02$ Å, and a coupling strength of $J_0 = 0.97 \pm 0.03$ GHz at $r_0 = 8.64$ Å (three lattice constants).

Chapter 4

The Lindblad Equation

This chapter explores two models which use the Lindblad equation for the decoherence of a multiple particle spin chain coupled to an electron bath. Recall the Lindblad equation:

$$\frac{\mathrm{d}\hat{\rho}}{\mathrm{d}t} = -\frac{i}{\hbar}[\hat{H},\hat{\rho}] + \sum_k \hat{L}_k \hat{\rho} \hat{L}_k^\dagger - \frac{1}{2}\sum_k \{\hat{L}_k^\dagger \hat{L}_k, \hat{\rho}\}. \tag{4.1}$$

The specific interaction with the environment is not required as the Lindblad equation incorporates all interactions in ladder operators. The first model uses the spin eigenbasis of the chain where the spin ladder operators act on individual atoms. The second model considers the effect of the environment on the energy eigenstates of the entire chain. To this end, energy ladder operators are used which act on the collective energy eigenstate. Note that the use of hats is dropped as notation for operators.

4.1. Model 1: Single Particle Decay

This chapter will derive the jump operators of a single atom based on the Pauli rate equations. The model uses the spin eigenbasis of the chain where the spin jump operators act on individual atoms. The jump operators of a single atom can be expanded to multiple atoms. A single spin-$\frac{1}{2}$ adatom subject to a magnetic field relaxes to the thermal equilibrium state in time T_1. Under certain approximations this can be modelled by the Pauli rate equations [9]. The following jump operators for the general Lindblad equation are such that they equal the Pauli rate equations:

$$L_+ = \sqrt{k_+} S_+, \tag{4.2}$$

$$L_- = \sqrt{k_-} S_-. \tag{4.3}$$

Here, S_+ and S_- are the spin jump operators; k_+ and k_- are the k-rates from the Pauli equations (derived previously in section 2.5.1), which can be expressed in terms of T_1 and other quantities:

$$k_+ = \frac{1}{1+e^{\frac{\hbar\omega}{k_B T}}} \frac{1}{T_1}, \tag{4.4}$$

$$k_- = \frac{1}{1+e^{\frac{-\hbar\omega}{k_B T}}} \frac{1}{T_1}. \tag{4.5}$$

Also, ω is the Zeeman splitting ($g\mu_B B$), T the temperature and T_1 the relaxation time. T_1 can be rewritten in terms of other physical quantities (G, the surface conductance and q the electric charge) as follows:

$$\frac{1}{T_1} = \frac{G\hbar\omega}{q^2} \frac{\sinh\frac{\hbar\omega}{k_B T}}{\cosh(\frac{\hbar\omega}{k_B T})-1} \left(= \frac{G\hbar\omega}{q^2} \frac{\cosh(\frac{\hbar\omega}{k_B T})+1}{\sinh\frac{\hbar\omega}{k_B T}} \right). \tag{4.6}$$

The jump operators include the decoherence as a result of energy loss. To include decoherence due to pure dephasing, a Lindblad term with pure dephasing operator is needed, given by:

$$L_\phi = \sqrt{\frac{1}{2T_\phi}} S_z, \tag{4.7}$$

with $T_\phi = \frac{2T_1T_2}{2T_1-T_2}$, where T_2 is the characteristic time of the total system decoherence, and T_1 is again the characteristic time of evolution to the equilibrium state.

Figure 4.1 depicts the exponential decay of the expectation value of S_x and S_z as a result of decoherence for one Ti atom. The Ti atom was initially in perfect superposition at $T = 1.2$ K and $B = 0.9$ T. The operators used in the Lindblad equation were as in Eqs. 4.2, 4.3, and 4.7, where the values used for T_1 and T_2 were 190 ± 50 ns and $95 \pm 15 \approx 100$ ns, respectively (found by Yang et al. [16]).

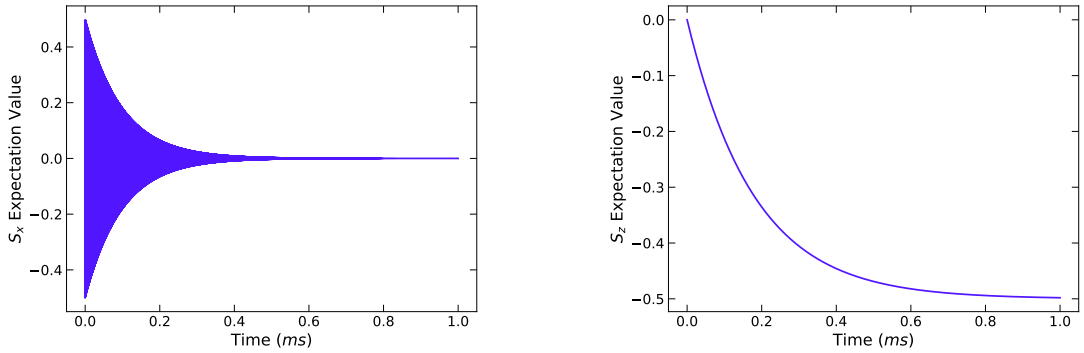

(a) Expectation value of S_x

(b) Expectation value of S_z

Figure 4.1: Time evolution of the expectation values of S_x and S_z for a Ti-atom initially in perfect superposition.

As a preliminary model for the flip-flop interaction of a spin chain coupled to an electron bath, the Lindblad equation with local jump operators is used. The local interaction strength is assumed the same as for a single atom. The local jump operators can be calculated by applying the tensor product (eq. 2.8) to the jump operators found above (eq. 4.3, 4.2, 4.7). The model is only realistic for very weakly coupled spin chains, since for strongly coupled spin chains the assumption of only local interaction is not valid. An important advantage of this model is that it easily scales up to multiple particle spin chains without increasing the computation time drastically. Note that it is necessary to know T_1 and T_2 from experiment. An advantage of the formulation of the ladder operators using T_1 and T_2 is that the exponential dependence on T of the jump operators is made clear (see eq. 4.4, 4.5) where T_1 acts as just a scaling factor.

Another way to express the Lindblad operators is by using the scaling factor J_{surf}, which represents the coupling strength of the Ti atom to the surface. In this way, a more insightful notation of the ladder operators is obtained since our second model will also depend on J_{surf}. The value of J_{surf} can be found through experiment, or in the case of Ti atoms at $B = 0.9$T and $T = 1.2$ K it's value can be found by letting the decoherence time correspond to T_2 that was found by Yang et al. [16]. Consider the following prefactor for the spin raising/lowering operator for a 2 atom system:

$$L_\pm^{(n)} = k_\pm^{(n)} S_\pm^{(n)}. \tag{4.8}$$

The index (n) of $L_\pm^{(n)}$ indicates that this spin operator works on the n^{th} atom. This is again determined by its position in the tensor product. For the dephasing operator, S_z, an extra factor of $\frac{1}{2}$ is introduced. For the prefactors we find:

$$\begin{aligned} k_{\pm,z}^{(n)} &= J_{\text{surf}}^2 \frac{1}{2^{N-1}} \sum_{i,j} \frac{\epsilon_{ij}}{e^{\frac{\epsilon_{ij}}{k_B T}} - 1} |\langle i| S_{\pm,z}^{(n)} |j\rangle|^2, \quad \text{if } E_i \neq E_j, \\ &= k_B T J_{\text{surf}}^2 \frac{1}{2^{N-1}} \sum_{i,j} |\langle i| S_{\pm,z}^{(n)} |j\rangle|^2, \qquad \text{if } E_i = E_j. \end{aligned} \tag{4.9}$$

The factor J_{surf} is the coupling strength of the atoms to the surface. The prefactor of the Lindblad operator depends on the different eigenstates $|i\rangle$ and $|j\rangle$, the energy differences, and the Boltzmann factor. The factor 2^{N-1} to accounts for double counting.

4.2. Model 2: Collective Spin Chain Decoherence

The second model considers the effect of the environment on the energy eigenstates of the entire chain. The environment interacts with the chain by means of a spin-scattering electron from the substrate that interacts with the adatoms, and returns to the substrate. [9] By making a diagonalization of the Hamiltonian: $H = PDP^\dagger$, with D a diagonal matrix of the energy eigenvalues, a density matrix in the spin eigenbasis ($\hat{\rho}_S$) can be expressed in the energy eigenbasis ($\hat{\rho}_E$) by using $\hat{\rho}_E = P^\dagger \hat{\rho}_S P$, and vice versa: $\hat{\rho}_S = P\hat{\rho}_E P^\dagger$. In this energy eigenbasis the eigenstates are the standard basis vectors, and n times degenerate eigenvalues appear n times on the diagonal matrix D, meaning different spin eigenstates are still distinct eigenstates in the energy basis. The convention that will be used is that the eigenvectors are assigned the lowest to highest eigenvalue respectively as:

$$\begin{pmatrix}1\\0\\\vdots\\0\end{pmatrix}, \begin{pmatrix}0\\1\\\vdots\\0\end{pmatrix}, \ \ldots, \ \begin{pmatrix}0\\\vdots\\1\\0\end{pmatrix} \begin{pmatrix}0\\\vdots\\0\\1\end{pmatrix}.$$

This means the energy ladder operators are $2^N \times 2^N$ matrices with a single nonzero entry of value 1 (N is the amount of particles in the system; for spin-1/2 particles this implies a 2^N dimension of the eigenstates). For example, the ladder operator used to jump from the lowest to second lowest energy eigenstate is:

$$E_{0\to 1} = \begin{pmatrix}0 & 0 & \ldots & 0\\1 & 0 & & 0\\0 & 0 & & 0\\\vdots & & \ddots & 0\\0 & 0 & \ldots & 0\end{pmatrix}.$$

The energy jump operators need the correct prefactor in the Lindblad equation:

$$L_{i\to j} = \sqrt{k_{i\to j}} E_{i\to j}, \tag{4.10}$$

where the notation $i \to j$ is used to indicate the transition between energy eigenstate $|i\rangle$ to $|j\rangle$. The transition rate $k_{i\to j}$ in this jump operator, as derived in section 2.5.1, is given as [9]:

$$\begin{aligned} k_{i\to j} &= \frac{\epsilon_{ij}}{e^{\frac{\epsilon_{ij}}{k_B T}} - 1} J_{\text{surf}}^2 \sum_{\sigma_k,\sigma_{k'}} \sum_{n=1}^{N} |\, \langle i\sigma_k | \boldsymbol{\sigma}\cdot\mathbf{S}^{(n)} | j\sigma_{k'}\rangle \,|^2, \quad \text{if } E_i \neq E_j, \\ &= k_B T J_{\text{surf}}^2 \sum_{\sigma_k,\sigma_{k'}} \sum_{n=1}^{N} |\, \langle i\sigma_k | \boldsymbol{\sigma}\cdot\mathbf{S}^{(n)} | j\sigma_{k'}\rangle \,|^2, \qquad \text{if } E_i = E_j. \end{aligned} \tag{4.11}$$

The composition of this transition rate can be viewed as follows. It starts with a Boltzmann factor depending on the temperature T and the difference in energy of the eigenstates ϵ_{ij}. Then the summation is over all the possible spin states of the scattering electron (σ_k and $\sigma_{k'}$). The operator $\hat{\sigma}\cdot\hat{S}$ is a dot product of the Pauli spin matrices and the spin operators in the $\hat{x}$, $\hat{y}$ and $\hat{z}$ direction. Then the projection of the joint state of the eigenstates $|i\rangle$ and $|j\rangle$ with all possible electron spin states are calculated. The factor J_{surf} is the coupling strength between the atoms and the substrate. Note that although $k_{i\to j}$ is a transition rate between two energy eigenstates, the states in the sum are calculated in the spin basis.

It is important to note that pure dephasing in this form of the Lindblad operators is not captured since it only considers energy jumps (relaxations and excitations). A pure dephasing operator would require a negative sign on the diagonal (recall from the S_z operator), which is not possible here.

Chapter 5

Analytical Solution

This chapter will delve into the analytical solution of the Lindblad equation for a system of two atoms. It will begin with an illustrative example which examines the relatively simple case of two atoms where the only interactions are decay and dephasing. Subsequently, an additional layer of complexity will be introduced by incorporating exchange interaction into the system. This will show how solving such equations becomes increasingly difficult as the system becomes more intricate.
Recall the Lindblad equation (eq. 2.25):

$$\frac{d}{dt}\rho = \frac{-i}{\hbar}[H,\rho] + L[\rho]. \tag{5.1}$$

In which H is the total Hamiltonian, and L is the Lindblad superoperator:

$$L[\rho] = \sum_k L_k \rho L_k^\dagger - \tfrac{1}{2}\sum_k \{L_k^\dagger L_k, \rho\}.$$

When considering the jump operators and the dephasing operator separately (spin basis, see Section 4.1), it is possible to divide this master equation into two differential equations for the diagonal and off-diagonal elements [10]:

$$\begin{aligned} \frac{d}{dt}\rho_{nn}(t) &= \frac{-i}{\hbar}[H,\rho(t)]_{nn} + (L_\pm[\rho])_{nn}, \\ \frac{d}{dt}\rho_{nm}(t) &= \frac{-i}{\hbar}[H,\rho(t)]_{nm} + (L_\pm[\rho])_{nm} - \gamma\rho_{nm}, \quad \text{if } n \neq m. \end{aligned} \tag{5.2}$$

With γ the prefactor as in eq. 4.9, and L_k in $L_\pm[\rho]$ the jump operators for individual atoms as defined in eq. 4.8. The term $\gamma\rho_{nm}$ for $n \neq m$ comes from the pure dephasing operator.

5.1. Two Particle System limited to Dephasing and Decay

Consider a system of two atoms where there is no exchange or dipolar interaction and no magnetic field. This illustrative example considers only interaction with the environment in the form of the dephasing operator L_ϕ and the decay operators $L_-^{(n)}$. The $L_+^{(n)}$ operator is intentionally omitted in order to obtain a relatively straightforward manual solution for the system. By doing so, this will help us understand the next example which is significantly more complex, while also providing us with preliminary insights into the general properties of the time-dependent solution. The system is considered in the high temperature limit, where all the prefactors of the Lindblad operators are the same and are denoted as γ. This will result in the following set of differential equations:

$$\begin{bmatrix} \dot\rho_{11} & \dot\rho_{12} & \dot\rho_{13} & \dot\rho_{14} \\ \dot\rho_{21} & \dot\rho_{22} & \dot\rho_{23} & \dot\rho_{24} \\ \dot\rho_{31} & \dot\rho_{32} & \dot\rho_{33} & \dot\rho_{34} \\ \dot\rho_{41} & \dot\rho_{42} & \dot\rho_{43} & \dot\rho_{44} \end{bmatrix} = \gamma \begin{bmatrix} \rho_{22}+\rho_{33} & -\rho_{12}+\rho_{34} & -\rho_{13}+\rho_{24} & -2\rho_{44} \\ -\rho_{21}+\rho_{43} & -\rho_{22}+\rho_{44} & -2\rho_{23} & -2\rho_{24} \\ -\rho_{31}+\rho_{42} & -2\rho_{32} & -\rho_{33}+\rho_{44} & -2\rho_{34} \\ -2\rho_{41} & -2\rho_{42} & -2\rho_{43} & -2\rho_{44} \end{bmatrix}. \tag{5.3}$$

Note that the dephasing operator L_ϕ causes only off-diagonal terms according to equation 5.2 where $\dot\rho_{nm} = -\gamma\rho_{nm}$. These entries in the density matrix where $\dot\rho_{nm} = -\gamma\rho_{nm}$ are easily solved as $\rho_{nm}(t) = \rho_{nm}(0)e^{-\gamma t}$. Now for the following subsystem of differential equations of the diagonal elements:

$$
\begin{aligned}
\dot{\rho_{11}} &= \gamma(\rho_{22} + \rho_{33}),\\
\dot{\rho}_{22} &= \gamma(-\rho_{22} + \rho_{44}),\\
\dot{\rho}_{33} &= \gamma(-\rho_{33} + \rho_{44}),\\
\dot{\rho}_{44} &= \gamma(-2\rho_{44}).
\end{aligned}
\tag{5.4}
$$

By substituting the solution $\rho_{44}(t) = \rho_{44}(0)e^{-2\gamma t}$, and using an integrating factor we obtain:

$$
\begin{aligned}
\rho_{22}(t) &= -\rho_{44}(0)e^{-2\gamma t} + \left(\rho_{22}(0) + \rho_{44}(0)\right)e^{-\gamma t},\\
\rho_{33}(t) &= -\rho_{44}(0)e^{-2\gamma t} + \left(\rho_{33}(0) + \rho_{44}(0)\right)e^{-\gamma t}.
\end{aligned}
\tag{5.5}
$$

These solutions can be used to obtain an expression for $\rho_{11}(t) = \rho_{44}(0)e^{-2\gamma t} - \left(\rho_{22}(0) + \rho_{33}(0) + 2\rho_{44}(0)\right)e^{-\gamma t} + \rho_{11}(0) + \rho_{22}(0) + \rho_{33}(0) + \rho_{44}(0)$. The final subsystem of equations that need to be solved is given by:

$$
\begin{bmatrix} \dot{\rho_{12}} \\ \dot{\rho_{13}} \\ \dot{\rho_{21}} \\ \dot{\rho_{31}} \\ \dot{\rho_{24}} \\ \dot{\rho_{34}} \\ \dot{\rho_{42}} \\ \dot{\rho_{43}} \end{bmatrix} = \gamma \begin{bmatrix} -1 & 0 & 0 & 0 & 0 & 1 & 0 & 0 \\ -1 & 0 & 0 & 1 & 0 & 0 & 0 & 0 \\ -1 & 0 & 0 & 0 & 0 & 0 & 0 & 1 \\ -1 & 0 & 0 & 0 & 0 & 0 & 1 & 0 \\ -2 & 0 & 0 & 0 & 0 & 0 & 0 & 0 \\ -2 & 0 & 0 & 0 & 0 & 0 & 0 & 0 \\ -2 & 0 & 0 & 0 & 0 & 0 & 0 & 0 \\ -2 & 0 & 0 & 0 & 0 & 0 & 0 & 0 \end{bmatrix} \begin{bmatrix} \rho_{12} \\ \rho_{13} \\ \rho_{21} \\ \rho_{31} \\ \rho_{24} \\ \rho_{34} \\ \rho_{42} \\ \rho_{43} \end{bmatrix}.
\tag{5.6}
$$

Given the many zero entries of this matrix it is straightforward to compute the eigenvectors $\mathbf{v}_i$ with corresponding eigenvalues λ_i, and then construct the solution as:

$$
\begin{bmatrix} \rho_{12} \\ \rho_{13} \\ \rho_{21} \\ \rho_{31} \\ \rho_{24} \\ \rho_{34} \\ \rho_{42} \\ \rho_{43} \end{bmatrix} = \sum_{i=1}^{8} = C_i e^{-\lambda_i t}\mathbf{v}_i.
\tag{5.7}
$$

Where the coefficients C_i are given by the initial conditions of the system. From this example, the exponential nature of the decoherence of a quantum system becomes evident. Notice also that if λ_i is complex, that is, where the oscillating terms in the density matrix originate from.

5.2. Decoherence of a Two Particle System with Exchange Interaction

Consider a dimer in the high temperature limit, where only the exchange interaction of both spins is considered. Our Hamiltonian is given by eq. 2.15. In the high temperature limit, all spin Lindblad operators have the same prefactor γ. These Lindblad spin-$\frac{1}{2}$ operators are given by:

$$
L_a^{(n)} = \gamma S_a^{(n)}.
\tag{5.8}
$$

With $a = \{x, y, z\}$, n denoting the atom on which the operator acts, and γ the prefactor. After substitution of these operators and writing out the matrix products in eq. 5.1, this can be rewritten as a system of differential equations:

$$
i\hbar\frac{d}{dt}\rho_v = U\rho_v.
\tag{5.9}
$$

Here U is the evolution matrix, and ρ_v is the density matrix reshaped as a vector (see 5.6 for an example). This system of ODE's can be solved by finding the eigenvalues and eigenvectors of U, and using the general solution given by:

$$
\rho_v = \sum_{i=1} = C_i e^{-\lambda_i t}\mathbf{v}_i.
\tag{5.10}
$$

Where the sum is applied to all eigenvalues $\mathbf{v}_i$. λ_i are the corresponding eigenvalues, and C_i constants to be determined by the initial conditions. The Python module *SymPy* can be used to solve for the exact solutions. Alternatively, since we are in the weak coupling limit where the prefactor is much smaller than the exchange coupling strength, i.e. $\gamma << J$, a leading order expression can be obtained for the solution by first-order Taylor expansion of λ_i and $\mathbf{v}_i$ around $\frac{\gamma}{J} = 0$ (again using *SymPy*). The full evolution matrix is given in the appendix Eq. A.

Initialising in up-down state gives the following evolution matrix (Energy basis):

$$\rho(t) = \frac{1}{4}\begin{bmatrix} 1-e^{-2\gamma t} & 0 & 0 & 0 \\ 0 & 1+e^{-2\gamma t} & -2e^{-\frac{3}{2}\gamma}\cos(Jt) & 0 \\ 0 & -2e^{-\frac{3}{2}\gamma t}\cos(Jt) & 1+e^{-2\gamma t} & 0 \\ 0 & 0 & 0 & 1-e^{-2\gamma t} \end{bmatrix}. \tag{5.11}$$

In this expression, $\gamma = \frac{1}{2}k_B T J_{surf}^2$ and J is the exchange coupling strength. In figure 5.1, the coherence $\rho_{23}(t) = \rho_{32}(t) = -\frac{1}{2}e^{-1.5\gamma t}\cos(Jt)$ is plotted for multiple values of temperature T.

Analytical Solution of Coherence for Different Temperatures

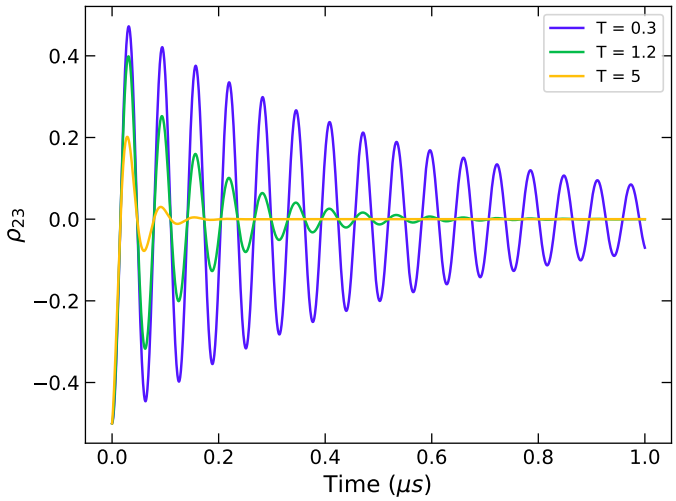

Figure 5.1: Analytical solution of the coherence: $\rho_{23}(t) = \rho_{32}(t) = -\frac{1}{2}e^{-1.5\gamma t}\cos(Jt)$. The analytical solution shown is obtained for two atoms initially in the up-down state.

Chapter 6

Results

In this chapter, the results obtained from the numerical implementation of the Lindblad equation are presented. These results show the outcomes for various scenarios using the two models of decoherence. The first model (Sec. 4.1) considers decay operators acting on individual spins. The second model (Sec. 4.2) uses Lindblad operators that act on the collective energy level of the spin chain. The alignment of these models with the findings of Yang et al. [16] for a single atom (Sec. 6.1) is demonstrated. Next, the analysis is extended to encompass two atoms, enabling a comparison of the models and uncovering similarities and differences, particularly with regard to exchange coupling. Following that, we delve into a current area of research that explores asymmetric coupling to the surface (Sec. 6.2). In this case, only one atom is subject to coupling with the surface. Our investigation will focus on understanding the temperature dependence of this system. Subsequently, the focus shifts to situations where our model demonstrates its greatest effectiveness: modelling configurations involving more than two spins. Specifically, the flip-flop oscillation of a chain of multiple atoms in section 6.3 is examined, triggered by flipping a single spin.Lastly, the combined situation of a multiple atom spin chain with asymmetric coupling, where only the first atom experiences coupling with the bath, is explored to consider the behaviour and properties of such configurations (Sec. 6.4).

6.1. Comparing both Models

In this first section, the alignment of the two models with the findings of Yang et al. [16] for a single atom is demonstrated. The variables employed by Yang include a magnetic field $B = 0.9$ T in the $[1,1,0]$-direction of the MgO crystal layer, a temperature $T = 1.2$ K, and a g-factor of $g = 1.98$. Subsequently, the situation is expanded to two atoms, where exchange interaction comes into play and results in some differences between the two models.

6.1.1. A Single Ti Atom

The time evolution of the Ti atom initially in perfect superposition of the magnetisation singlet and triplet states (therefore resulting in up-down initial state) was done for the first model with operators in the spin basis according to the analytic method of section 4.1, and for the second model in the energy basis with the method of section 4.2. Recall that the variable J_{surf} represents the atom's coupling to the surface, and functions as a scaling factor for the decoherence. The larger the coupling with the surface, the faster the system decoheres.

In figure In figure 6.1, the time evolution of the density matrix is depicted. The graphs of the second model are shown since no significant difference is observed for both models in this case. An exponential decay relation $Ae^{Bt} + C$ (where A, B, and C are constants to be determined according to the fit) is fitted to the diagonal element. A decoherence time corresponding to Yang et al. [16] of $\frac{1}{B} = 190$ ns is obtained when using a surface coupling of $2 \cdot 10^{-2}$ MHz = 20 kHz.

6.1.2. Two Ti Atoms

The setup of the two atom system is depicted in figure 6.2. The oxygen bound Ti atoms are separated by a separation vector $\vec{r}$, which has a length of three lattice constants (8.64 Å). The strength of the exchange coupling with respect to the interactomic distance, deduced using eq. 3.2, is $J = 970$ MHz. The magnetic field,

Single Ti atom on a Surface

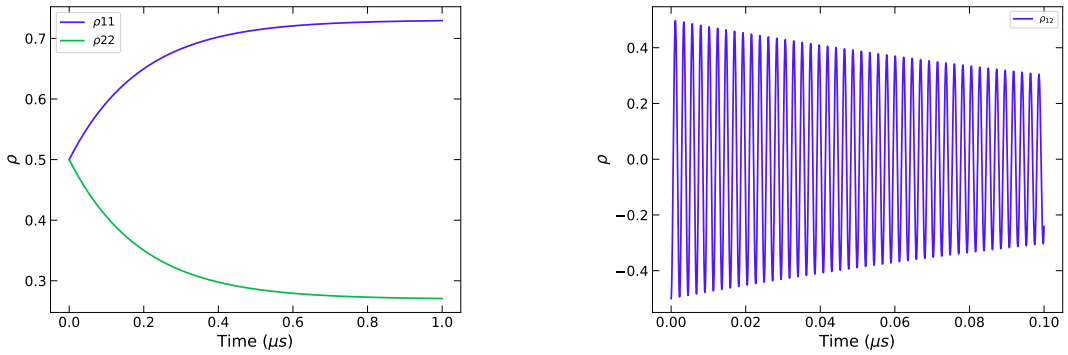

(a) Occupations

(b) Coherences

Figure 6.1: Time evolution of the density matrix for a Ti-atom initially in perfect superposition. (a): Occupations of energy eigenstates, (b): Coherences, where $\rho_{12} = \rho_{21}^*$, and the timescale is shortened to show the oscillations.

as mentioned before, has a direction of $[1,1,0]$ and forms an angle of $\theta = \frac{1}{4}\pi$ with $\vec{r}$. This results in a dipolar coupling strength of $D = 20$ MHz, as given by eq. 2.14, with $D_0 \approx 80$ MHz [16].

Visualisation of Two Ti Atoms on a Surface

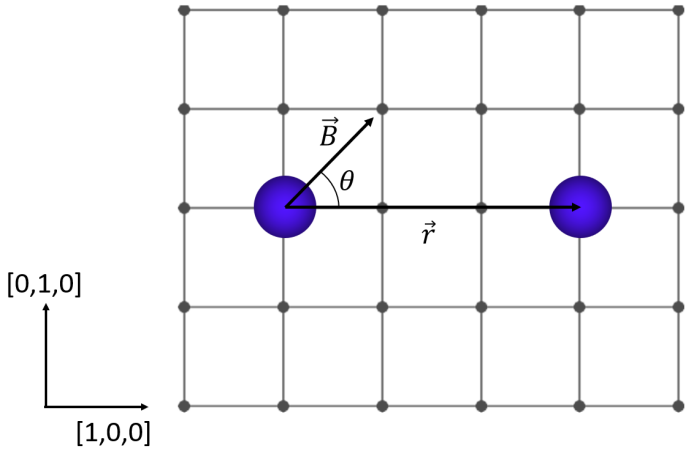

Figure 6.2: Two Ti atoms on the MgO lattice represented by the grid (the lattice constant is 2.88Å). $\vec{r}$ is the separation vector, $\vec{B}$ the magnetic field and θ is the angle between them.

In figure 6.3 the results of the two models for the decoherence are shown for two atoms initially in the state up-down. Where figure (a) used an exchange coupling of 970 MHz, and figure (b) used an exchange coupling a factor 10 larger ($J = 9700$ MHz). It was verified that the final state of both models equals the Boltzmann equilibrium state in figure (a), and also for the full-chain decoherence model in figure (b). The density matrix is shown in the energy basis.

When comparing figures (a) and (b) from Fig. 6.3, the distinction between both models becomes evident as the time evolution of the diagonal entries of the density matrix is not identical for the large value of J. Model 1 incorporates spin ladder and dephasing operators in the Lindblad equation, reflecting the influence of the environment on atoms through spin flipping in the Kondo interaction. This process is captured by individual spin ladder and dephasing operators that act on the atom's spin state (as discussed in Section 4.2). However, in the presence of exchange interaction, the assumption of individual interactions is not entirely valid due to the coupling between the atoms. In contrast, Model 2 employs energy ladder operators that act on the collective state, thus not assuming this individual interaction. Hence, it should be noted that for very large exchange

coupling, the single-atom decoherence model might be less reliable.

Comparing both Models w.r.t Exchange Coupling J for a Ti dimer

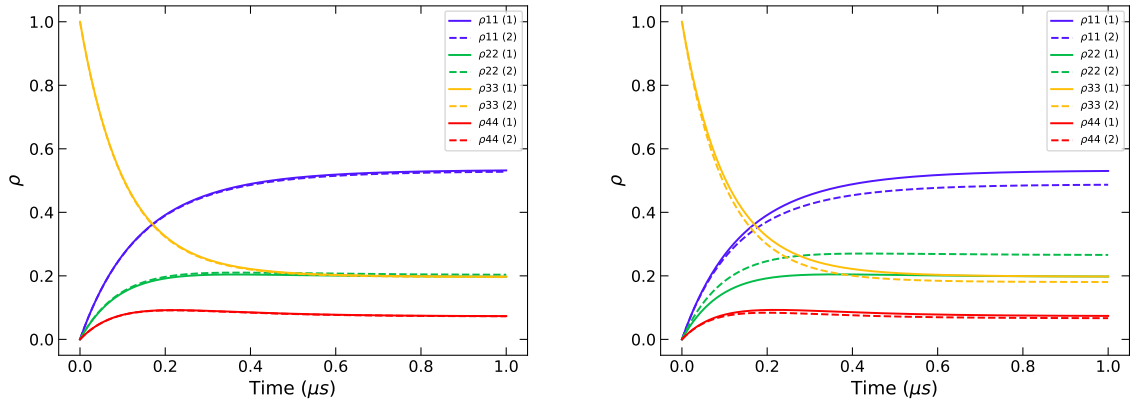

(a) Occupations (J = 970 MHz)

(b) Occupations (J = 9700 MHz)

Figure 6.3: Time evolution for two Ti-atoms initially in the up-down state. The density matrix is represented in the energy basis for both figures, where ρ_{ii} is the occupation of energy eigenstate $|i\rangle$ and (1), (2) denote the single particle decoherence model (solid line) and collective spin-chain decoherence (dashed line), respectively. For a large exchange coupling in figure (b), the distinction between both models can be seen. Model 2, which considers Lindblad operators acting on the energy levels, was validated to still approach the thermal equilibrium state.

6.2. Asymmetric Coupling to the Surface

A current field of research involves situations where only one atom of a dimer experiences coupling with the surface while the other atom does not. The focus is on studying the coherences of this system, specifically the temperature dependency of their decoherence process, as there is no analytical solution available in this situation. In Section 5.2, the analytical solution was derived for a two atom system initially in the up-down state under the assumption of high temperature limit and considering only exchange interaction. The time evolution of the coherence between the second and third eigenstate (the triplet and singlet states) was deduced as follows:

$$\rho_{23}(t) = \rho_{32}(t) = -\frac{1}{2}e^{-1.5\gamma t}\cos(Jt). \tag{6.1}$$

In this equation, J is the exchange coupling strength and $\gamma = \frac{1}{2}k_B T J_{\text{surf}}^2$. This solution was obtained analytically in the high temperature limit as the prefactors γ in the Lindblad operators are all the same in this case. Now, our model comes into play when considering lower temperature situations where the prefactors will differ. The analytical model considered only exchange coupling, hence a magnetic field of 10 mT and an exchange coupling of 100 MHz were used, ensuring that the Zeeman splitting ($g\mu_B B$) is much smaller than J. This provides a sufficiently large splitting of the eigenvalues while still allowing the utilisation of the obtained equation.

In Figure 6.4(a), the time evolution of the density matrix element ρ_{23} (in the energy basis) is presented for multiple temperature values ($T = 0.3, 1.2, 5$ K) using the full-chain decoherence model (Model 2). The results from the single-atom decoherence model yield nearly identical outcomes, as anticipated from Section 6.1.2. Both symmetric coupling (where both atoms experience the same surface coupling J_{surf}) and asymmetric coupling (where only one atom is coupled to the surface with strength J_{surf}) are shown. The oscillatory behaviour characterised by a cosine function combined with exponential decay is clearly observed. Additionally, when comparing symmetric and asymmetric coupling at the same temperature, it is evident that the asymmetric dimer exhibits a lower decay rate. This can be attributed to the realisation that the Kondo interaction with the surface is the underlying cause of decoherence for both systems, with only one atom in the asymmetric dimer experiencing this interaction, this explains the reduced decay rate

In figure 6.4(b), the results of fitting ρ_{23} to the relation $y_{\text{fit}} = Ae^{-Bt}\cos(Ct) + D$ are presented, and the value of the exponential decay rate (denoted as B) is divided by $\frac{1}{2}k_B T J_{\text{surf}}^2$. It has been verified that for all temperature

Asymmetric and Symmetric Coupling vs. Analytical Solution

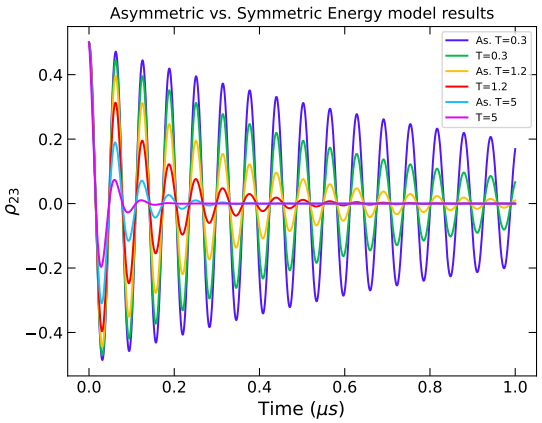

(a) Time evolution of coherence ρ_{23} for multiple values of T

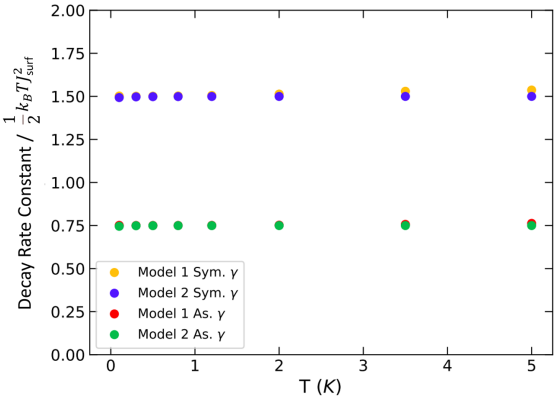

(b) Value of the decay rate constant divided by $\frac{1}{2}k_B T J_{\text{surf}}^2$ from the fit of ρ_{23} to eq. 6.1

Figure 6.4: Figure (a): Results for the time evolution of the density matrix element ρ_{23} (Energy basis) from the full-chain decoherence model (Model 2) for multiple values of temperature T (T = 0.3, 1.2, 5 K). The two Ti-atoms were initially in the up-down state, and have $J = 100$ MHz, $D = 0$, $B_z = 10$ mT. Both symmetric coupling (where both atoms experience the same surface coupling J_{surf}), and asymmetric coupling (where only one atom is coupled to the surface with strength J_{surf}) are considered. Figure (b): Results for fitting ρ_{23} to eq. 6.1 for both models (single-atom decoherence model (1) and full-chain decoherence model (2)), for multiple values of temperature T (T = 0.1, 0.3, 0.5, 0.8, 1.2, 2, 3.5, 5 K). This graph shows a linear dependence of the decay rate with temperature.

values T, A is approximately 0.5, C is approximately 100 (equal to J), and D is approximately 0, thereby conforming to our analytical model described in eq. 6.1. In the case of the symmetric model, a decay rate of 1.5γ is observed, which also aligns with our analytical model. In the case of the asymmetric model, the decay rate is half of that, specifically 0.75γ

Now, attention is turned to lower temperature values, where the analytical model might not be applicable as the approximation of nearly equal prefactors in the Lindblad equation no longer holds. A logarithmic scale with 10 steps was used to consider temperatures ranging from 0.1 mK to 100 mK. The same initial state and initial values as before were used, and both models for symmetric and asymmetric coupling were considered. Results are shown in figure 6.5. In figure 6.5, it can be seen that the behaviour of the density matrix element ρ_{23} no longer follows the analytical solution given by eq. 6.1. Namely, for very small temperatures, the decay rate far exceeds 1.5γ. Note that in Figure 6.5, the y-axis is restricted to get a more detailed view of the temperature-dependent behaviour. It can be seen for a temperature less than roughly 20 mK, the analytical model breaks down. Also, for those temperatures, there are slight differences between model 1 and 2. This might be explained since the decay rate for small temperatures is so little, that fitting the results to the relation $\gamma_{\text{fit}} = Ae^{-Bt}\cos(Ct) + D$ induces a small-scale error since the decay term is almost constant, hence small differences between both models are amplified. Also, for lower temperatures, the exchange coupling becomes relatively large in comparison, hence resulting in the same dissimilarities previously seen in Sec. 6.1.2 caused by assumption of individual interaction in the first model.

6.3. Flip-Flop Oscillation for a Multiple Atom Chain

This section will analyse the flip-flop oscillation of a multiple particle chain. When considering a chain of atoms in an external magnetic field, flipping a single atom will result in a flip-flop oscillation of the spin expectation values. The flip-flop oscillation refers to the oscillatory exchange of spin states between adjacent particles in the chain.

Under certain conditions, the particles' spins can undergo a periodic flipping motion, where the spin state of one particle changes while the spin state of its neighbouring particle simultaneously flips in the opposite direction (in the case of antiferromagnetic coupling). This exchange of spin states continues to propagate along the chain, leading to a collective oscillation that can persist for a certain period. The underlying mechanism behind the flip-flop oscillation lies in the coupling between the spins of neighbouring particles and their interaction with the external magnetic field. The magnetic field acts as a driving force that induces a predilection

Asymmetric and Symmetric Coupling for Small Temperatures

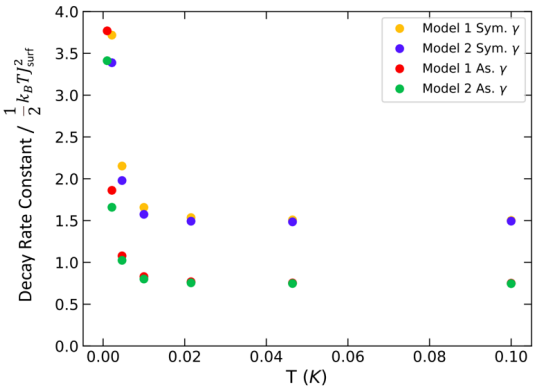

Figure 6.5: Results for fitting ρ_{23} to eq. 6.1 for both models (single-atom decoherence model (1) and full-chain decoherence model (2)), for multiple values of temperature T (T ranging from 0.1 mK to 100 mK on a logarithmic scale with 10 steps).

of the spin orientations, while the interactions such as dipolar and exchange coupling between adjacent spins provide a means for spin transfer. In figure 6.6, an illustration of this behaviour is depicted.

The flip flop oscillation of spin-1/2 chains has attracted significant interest due to its potential applications in various fields. It holds promise for applications in quantum computing, where spin chains can be harnessed for quantum information processing and quantum gate operations. Moreover, the phenomenon is relevant for studying quantum magnetism and many-body physics, shedding light on the fundamental quantum mechanical properties [15].

Flip-Flop Oscillation for a Chain of Four Atoms

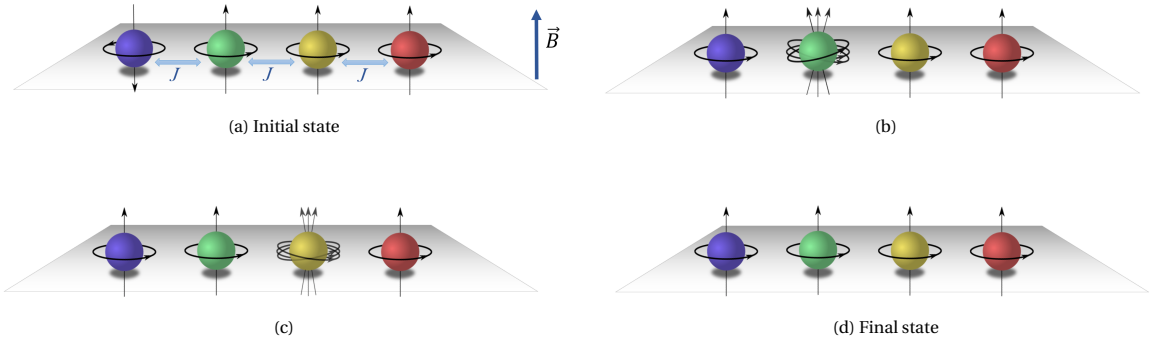

Figure 6.6: Flip-flop Oscillation of a chain consisting of 4 particles. The (strong) magnetic field is pointing upwards, meaning the spin of the atoms will have a preferred upward direction as well. The surface the atoms reside on represents the MgO lattice. The atoms are coupled with exchange coupling J. Figure (a): The initial state, where the first spin is flipped antiparallel to the magnetic field. Figure (b): Flipping the first atom causes the second atom to oscillate. For simplicity, the (smaller) oscillations of the other atoms are not depicted. Figure (c): Flip-flop oscillation of the third atom caused by exchange coupling between the neighbouring left atom. Figure (d): The chain has returned to it's equilibrium state.

There are certain conditions for this so-called flip-flop oscillation to occur. First of all, there needs to be a coupling between the atoms. In the case of a chain of Ti atoms, this is realised by the exchange and dipolar interaction. Also, the atoms need to have almost the same level splitting and thus Larmor frequency. To this end, all Ti atoms are considered oxygen-bound in this model, resulting in the same g-factor. Furthermore, the initial state must be an entangled state for the flip-flop evolution to occur. Lastly, the characteristic time of the system must be larger than the period of the oscillation.

To realise the conditions mentioned above, our system is prepared in an initial state where only the first atom has a spin orientation antiparallel to the magnetic field (spin down). The magnetic field is strong, namely a

value of 0.9 T such that the final state will be almost equal to all spins parallel to the magnetic field (spin up). The temperature of the heat bath considered is a low value of 300 mK. The exchange coupling is chosen to be 12 MHz (corresponding to an interatomic distance of 3 lattice constants (8.64 Å) in the x-direction and 2 lattice constants (5.76 Å) in the y-direction, see eq. 3.2). This exchange coupling results in only nearest-neighbour spin flipping. Furthermore, if the magnetic field is approximately parallel to the spin chain, the dipolar coupling is negligible (eq. 2.14).

In figure 6.7, results are shown for chain lengths varying from 2 to 7 atoms. As can be seen in all graphs, the initial expectation value of S_z is $-\frac{1}{2}$ for only the first atom (spin down) and $+\frac{1}{2}$ for all the other atoms (spin up). Then, consecutively, the other spins in the chains are also flipped. The decaying nature of the chain can be observed, where due to the interaction with the heat bath, it returns to the equilibrium state after a certain time.

In the appendix figure A.1, results are shown for both models. There are some minor distinctions between both models, the most notable being that a result of the individual interactions in the first model might be visible. Namely, in the full-chain decoherence model, the graphs for the atoms further off in the chain are more sloped at the start. This could mean that because our ladder operators are acting on the spin chain as a whole, the other atoms experience the flipping simultaneously. Whereas on the other hand, in the single-atom decoherence model, flipping happens individually and in a subsequent manner.

Another interesting observation is that for all chain lengths, the last atom in the chain experiences more oscillation than the atom before it (mostly visible in $N = 3,4,5,6$). An explanation for this could be that, since it is the last atom in the chain, it is only coupled to one other atom, hence resulting in more oscillation freedom.

Also, for the full chain decoherence model up to a chain length of 8 atoms, some oscillating coherences were plotted (see Appendix A.2) and fitted to the relation $y_{\text{fit}} = Ae^{-Bt}\cos(Ct) + D$, which reflects the exponential nature of the decay and oscillating term of the flip-flop interaction. The characteristic times ($\frac{1}{B}$) are plotted in figure 6.8. There is an almost steady decline in decoherence time with increased length of the chain. It was also verified that for higher values of exchange coupling, there was no significant difference in the chain length vs. decoherence time (within the uncertainty margin).

In the single particle decay model, the relation mentioned above for y_{fit} was found to be inadequate in accurately describing the system. This is because the oscillation of atoms higher up in the chain initiates at a later time, which is not considered in the cosine term. As a result, the graph displayed increased dispersion in decoherence time. However, despite this limitation, the system did exhibit similar behaviour.

Flip-Flop Oscillation for a Range of Particle Chain Lengths

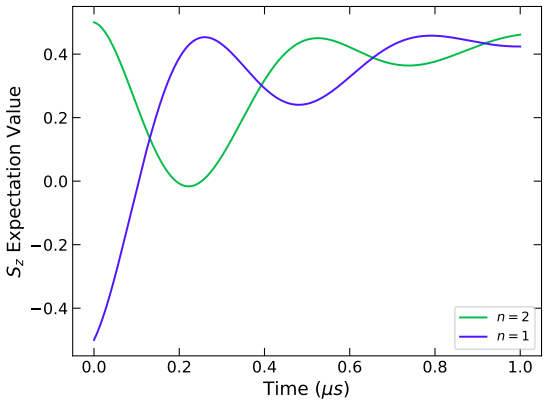

(a) N=2

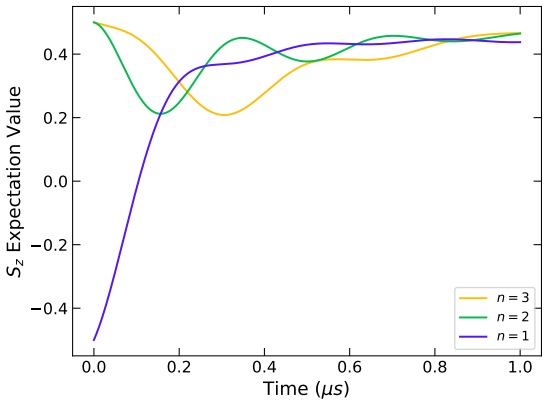

(b) N=3

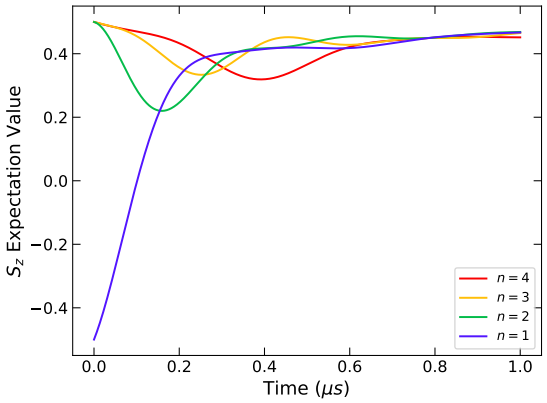

(c) N=4

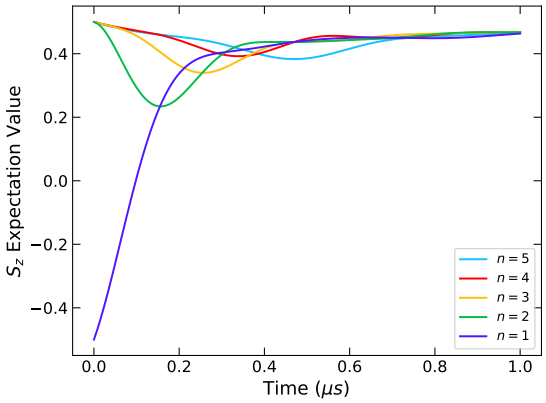

(d) N=5

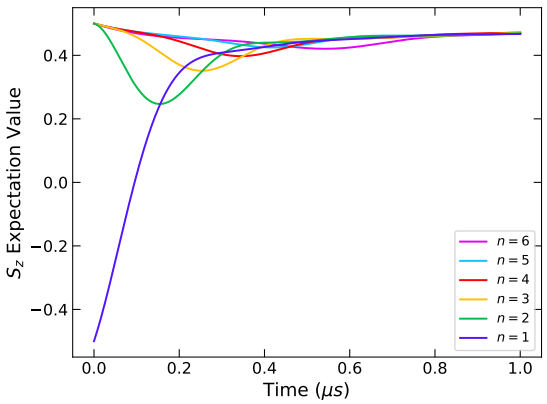

(e) N=6

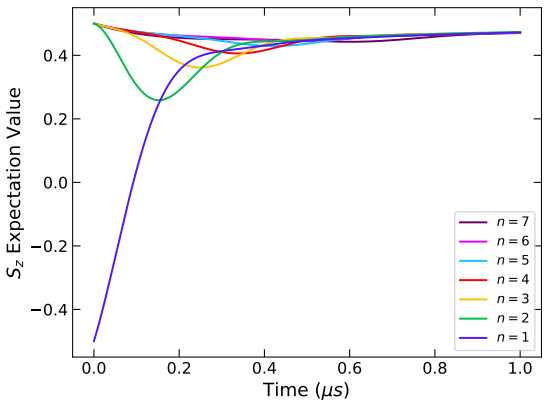

(f) N=7

Figure 6.7: Flip-flop Oscillation in S_z expectation value for a multiple atom chain with lengths ranging from 2 to 7 atoms (denoted by the number of atoms N). The magnetic field considered is 0.9 T, directed along the chain. The exchange coupling J is 12 MHz, and temperature $T = 300$ mK. Each time, only the first atom has orientation antiparallel to the magnetic field (spin down). The final state is all spins directed along the magnetic field. The results were obtained using the second model with collective spin chain decoherence.

Chain Length vs. Decoherence Time

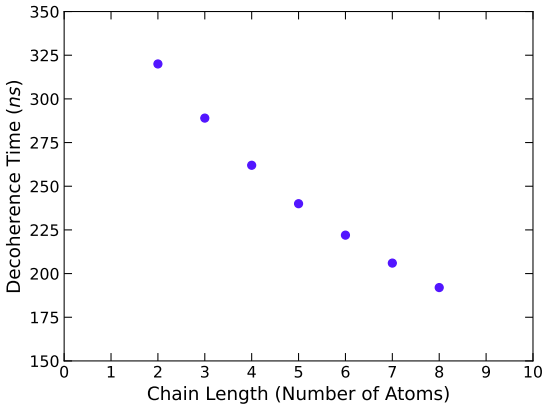

Figure 6.8: Relation between the decoherence time and length of the chain in number of atoms for the flip-flop oscillation ($J = 12$ MHz, $B = 0.9$ T, $T = 0.3$ K). Results were obtained using the second model with collective spin chain decoherence.

6.3.1. Higher Exchange Coupling for Three Atoms

The final flip-flop oscillation with symmetric coupling will be analysed is a case involving three atoms with a higher exchange coupling strength ($J = 100$ MHz). The three initial states under consideration are $|\uparrow\downarrow\downarrow\rangle$, $|\downarrow\uparrow\downarrow\rangle$, and $|\downarrow\downarrow\uparrow\rangle$, as shown in figure 6.9. It is interesting to observe that the modes of oscillation differ depending on which atom undergoes a spin flip.

When the middle atom is flipped, the situation becomes symmetric, resulting in both outer atoms exhibiting the same sinusoidal time evolution. However, when one of the outer atoms is flipped, the time evolution becomes more complex and is characterised by the presence of two distinct modes. The first mode being when the first atom flips only the second one, and the second mode being when the first atom causes the second and third atom to flip simultaneously.

Flip-Flop Oscillation with Different Oscillation Modes

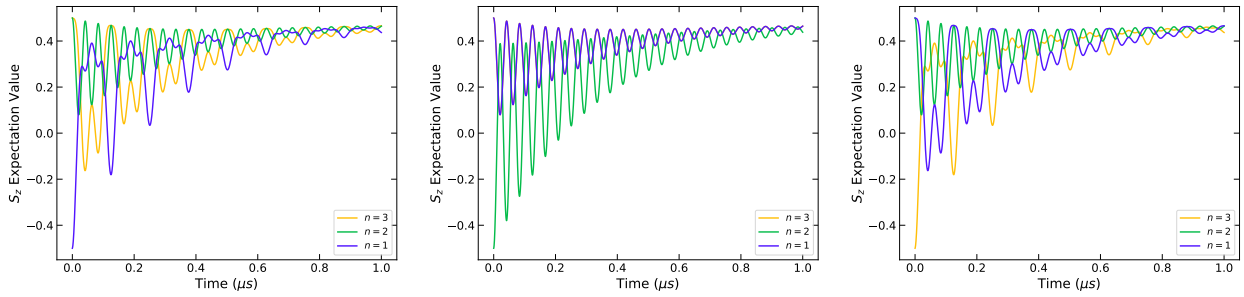

(a) Initial State $|\uparrow\downarrow\downarrow\rangle$ (b) Initial State $|\downarrow\uparrow\downarrow\rangle$ (c) Initial State $|\downarrow\downarrow\uparrow\rangle$

Figure 6.9: For a higher exchange coupling of $J = 100$ MHz, multiple oscillation modes are visible (a superposition of cosines) depending on the initial state. ($B = 0.9$ T, $T = 0.3$ K)

6.4. Flip-Flop Oscillation for a Chain of Atoms with Asymmetric Coupling

In this final section, the behaviour of a multiple atom spin chain is investigated, where only the first atom is coupled to the bath. It focuses on flip-flop oscillation, which occurs when the first atom (the one coupled to the bath) flips anti-parallel to the direction of the magnetic field. The magnetic field has a strength of 0.9 T, and the heat bath temperature is 300 mK. To ensure one mode of spin flipping without other oscillation modes, the exchange coupling is set to 12 MHz.

Flip-Flop Oscillation for a Range of Particle Chain Lengths for Asymmetric Coupling

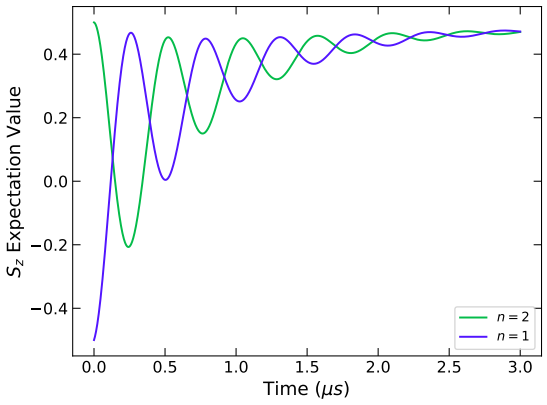

(a) N=2

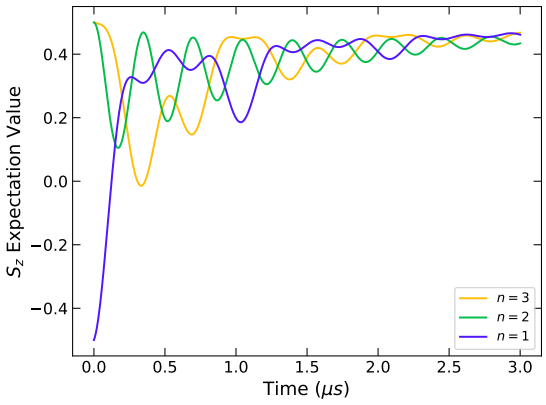

(b) N=3

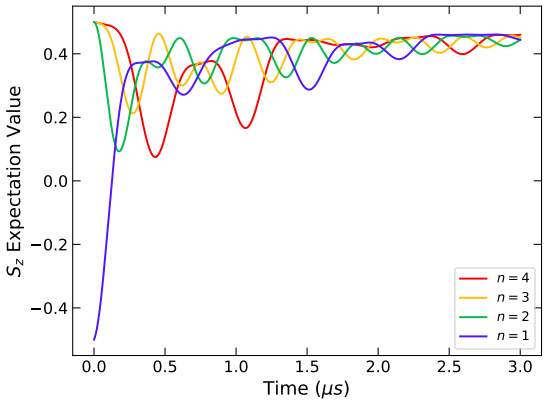

(c) N=4

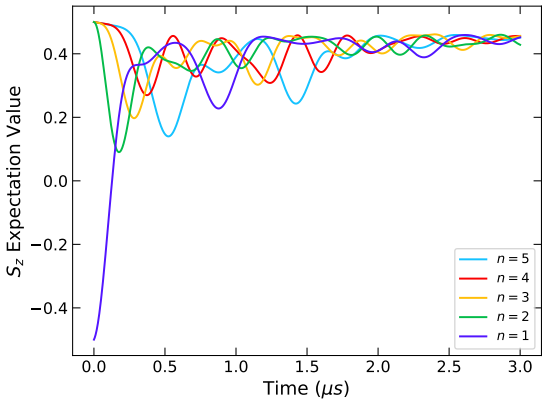

(d) N=5

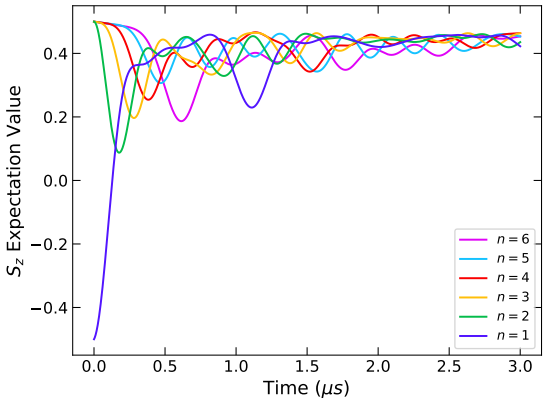

(e) N=6

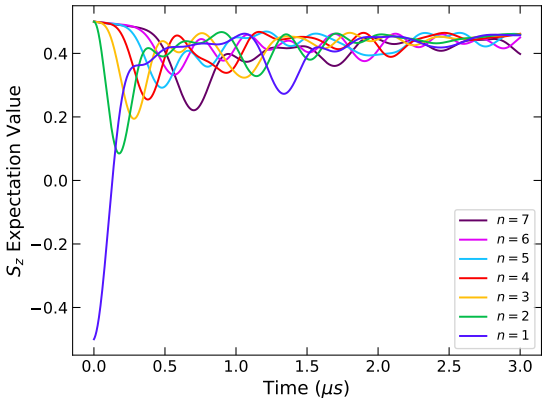

(f) N=7

Figure 6.10: Flip-flop Oscillation in S_z expectation value for a multiple atom chain with lengths ranging from 2 to 7 atoms (denoted by the number of atoms N). Only the first atom experiences coupling with the bath. The magnetic field considered is 0.9 T, directed along the chain. The exchange coupling J is 12 MHz, and temperature $T = 300$ mK. Each time, only the first atom has orientation antiparallel to the magnetic field (spin down). The final state is all spins directed along the magnetic field.

To implement asymmetric coupling in the model, prefactor of the Lindblad operators are modified (eq. 4.11) by summing only over the first atom instead of all N atoms. Figure 6.10 illustrates the results for chain lengths ranging from 2 to 7 atoms. In all the graphs, the initial expectation value of S_z is indeed $-\frac{1}{2}$ for the first atom (spin down) and $+\frac{1}{2}$ for the remaining atoms (spin up). As a result of this initialisation, the other spins in the chain are flipped consecutively. The graphs also exhibit the decaying nature of the chain, where it returns to the equilibrium state over time due to interaction with the heat bath. It was verified that the chain returns to the Boltzmann equilibrium state.

Comparing these results with those obtained from symmetric coupling, a similar behaviour but with less decoherence in the case of asymmetric coupling can be observed. For two atoms, the coherence time in the asymmetric case is twice as long as the symmetric coupling situation (Sec. 6.2). This can be attributed to the fact that only the first atom in the chain introduces decoherence, whereas in the symmetric case, adding an atom to the chain introduces an additional source of decoherence. Additionally, notice that the outer atoms of the chain experience more pronounced oscillations. Regarding the decoherence time, there was a notable dispersion in the values across different coherences, hence a definite conclusion about the relation between decoherence time and chain length cannot be drawn. One notable observation is that the decay rate of the chain does not notably decrease as the length increases.

However, it is crucial to acknowledge that the use of the secular approximation likely introduces a significant error in the case of asymmetric coupling. It has been demonstrated by Broekhoven [2] for a dimer that the largest discrepancy occurs when the two atoms have unequal coupling strengths to the surface. This mismatch causes the interaction to become too strong for the secular approximation to remain valid.

The implementation of asymmetric coupling to a chain with more than two atoms for the first model with single spin decay poses an ongoing challenge. One initial solution that comes to mind is to focus solely on the ladder operators that act on the first atom. However, it was verified that the chain does not evolve back to the Boltzmann equilibrium state in this approach. This method is likely to result in miscalculations since it fails to account for the influence of exchange coupling that is reflected in the prefactors of these operators. Obtaining results using the first model, which utilises individual spin operators, would be valuable since the interaction with the bath also occurs at the first individual atom. For this same reason, it is also questionable whether the collective spin chain decoherence model is the right approach for asymmetric coupling.

Chapter 7

Conclusions and Discussion

This thesis marks the initial steps towards modelling the decoherence process of a multi-atom chain on a conducting surface. Two models based on the Lindblad equation were employed: one considering decay operators acting on individual spins, and the other utilising operators acting on the collective state of the spin chain.

The primary focus of this study was on Ti atoms on MgO on Ag[001], which are bound to oxygen atoms and exhibit an effective spin-$\frac{1}{2}$. The Kondo interaction with the surface was identified as the main source of decoherence. The initial investigations involved a single atom, with the results compared to the findings of Yang et al. [17], including experimental values of decoherence and relaxation times. The subsequent step involved implementing a model for the surface scattering electrons mediating the Kondo interaction, as proposed by Loth et al. [9]. This model incorporated a scaling factor, J_{surf}, to account for the decoherence based on experimental data. While this rescaling provided a reasonable estimation for the total dimer evolution since the interaction with the STM tip is also of the Kondo interaction type, a significant improvement could be achieved by considering the interaction with the STM tip atom (thereby eliminating the need for rescaling).

7.1. Comparing the two Models for a Ti Dimer

The next stage involved comparing the two models for various exchange coupling strengths. The first model, employing individual spin operators, considers the interaction of the environment with the system as individual atom interactions. On the contrary, the second model employs collective spin chain operators, rendering it more reliable in the case of relatively high exchange coupling. This was verified by observing that the second model still converges to the Boltzmann equilibrium state in this case.

Another distinction between the models is the absence of pure dephasing in the collective spin chain decoherence model. The formulation of the prefactors for energy-level jump operators prevents their representation as pure dephasing operators. One possible solution could involve multiplying $E_{i\to i}$ by the sign of $\langle i|\, S_z^{(n)}\, |i\rangle$. However, this approach may necessitate rescaling or additional adjustments, and its feasibility has not yet been established.

7.1.1. Asymmetric vs. Symmetric Coupling to the Surface

Continuing the analysis, a Ti dimer was examined and the results were compared with the analytical solution presented in Ch.5 across a range of temperatures. The analytical solution relied on the high temperature limit, where all Lindblad prefactors could be approximated as identical. It was observed that both models (with exchange coupling in the range where the assumption of individual interaction of the first model is applicable) were in agreement with this analytical solution, except for very low temperatures, where the analytical solution was not applicable. This analytical solution included a linear dependence of the decay rate with temperature. Additionally, asymmetric coupling, where only one atom experiences interaction with the surface, resulted in a coherence time twice as long as that of the symmetric coupling case.

7.2. Flip-Flop Oscillation of a Multiple Spin Chain

To explore the more extensive applications of the models, the flip-flop oscillation of a multi-particle chain was investigated. Sequential flip-flop oscillation of atoms within the chain was observed by initiating the process

with the first atom. The relationship between the decoherence time and the length of the chain was plotted, showing a steady decline in decoherence time with an increased chain length, although the limited data points prevented drawing a definitive conclusion about the exact relation. Further research is necessary, either by utilising more computational power or improving the code to accommodate calculations for more atoms. Additionally, enhancing the accuracy of the models by incorporating more interactions and reducing approximations is also recommended. Namely, both models rely on the secular approximation. It has been demonstrated by Broekhoven [2] that the largest discrepancy occurs for a dimer when the two atoms have unequal coupling strengths to the surface. This mismatch causes the interaction to become too strong for the secular approximation to remain valid. Nonetheless, this effect is only significant in cases of substantial mismatch. Therefore, it can be assumed that the secular approximation holds in the scenario of symmetric coupling to the surface. However, it is important to note that the use of secular approximation likely introduces a significant error in the case of asymmetric coupling.

7.2.1. Asymmetric Coupling

For the case where only the first atom was coupled with the surface (using the second model with collective spin chain decay) a similar time evolution was observed as in the symmetric flip-flop case but with larger coherence time. Adding atoms to the chain did not seem to decrease coherence time. This is attributed to the fact that only the first atom introduces decoherence, whereas adding atoms in the symmetric case introduces additional sources of decoherence. Implementing asymmetric coupling to chains with more than two atoms remains a challenge, especially for the first model with individual spin decay, and alternative approaches are necessary to accurately model asymmetric coupling effects. Since the effect of decoherence from the bath is isolated to the first atom, it would be particularly interesting to explore the model with individual spin decay.

7.3. Further Research and Recommendations

As previously mentioned, extending the chain length is essential for drawing conclusions about the relationship between decoherence time and chain length. Furthermore, the current model should be expanded to include the interaction of the STM's tip atom, as well as the consideration of a time-dependent magnetic field caused by ESR-STM. Another improvement could involve employing the Bloch-Redfield equation, which assumes slightly weaker approximations than the Lindblad equation. Especially for the asymmetric coupling case, Bloch-Redfield offers a potential solution for mitigating the error caused by the strong secular approximation. Exploring different atom configurations would also be an interesting avenue for future research.

Bibliography

[1] Susanne Baumann, William Paul, Taeyoung Choi, Christopher P. Lutz, Arzhang Ardavan, and Andreas J. Heinrich. Electron paramagnetic resonance of individual atoms on a surface. *Science*, 350(6259):417–420, 10 2015. ISSN 10959203. doi: 10.1126/SCIENCE.AAC8703/SUPPL{_}FILE/BAUMANN.SM.PDF.

[2] R. Broekhoven. Models for probing the coherent free flipflop evolution of atomic effective spin 1/2 dimers with a tunneling microscope, 2020.

[3] C. Cohen-Tannoudji, J. Dupont-Roc, and G. Grynberg. *Atom-Photon Interactions: Basic Processes and Applications*. John Wiley & Sons, Inc, 1998. ISBN 978-0-471-29336-1.

[4] J. C. Cordes. The secular approximation with dipole-dipole interaction. *Journal of Physics B: Atomic and Molecular Physics*, 20(7):1433, 4 1987. ISSN 0022-3700. doi: 10.1088/0022-3700/20/7/012.

[5] F. Delgado and J. Fernández-Rossier. Spin decoherence of magnetic atoms on surfaces. *Progress in Surface Science*, 92(1):40–82, 2 2017. ISSN 0079-6816. doi: 10.1016/J.PROGSURF.2016.12.001.

[6] J. R. Johansson, P. D. Nation, and Franco Nori. QuTiP 2: A Python framework for the dynamics of open quantum systems. *Computer Physics Communications*, 184(4):1234–1240, 4 2013. doi: 10.1016/J.CPC.2012.11.019.

[7] Kreuzer and H. J. Nonequilibrium thermodynamics and its statistical foundations. *oxny*, 1981.

[8] Sebastian Loth, Markus Etzkorn, Christopher P. Lutz, D. M. Eigler, and Andreas J. Heinrich. Measurement of fast electron spin relaxation times with atomic resolution. *Science*, 329(5999):1628–1630, 9 2010. ISSN 00368075. doi: 10.1126/SCIENCE.1191688/SUPPL{_}FILE/LOTH.SOM.PDF.

[9] Sebastian Loth, Kirsten Von Bergmann, Markus Ternes, Alexander F. Otte, Christopher P. Lutz, and Andreas J. Heinrich. Controlling the state of quantum spins with electric currents. *Nature Physics 2010 6:5*, 6(5):340–344, 3 2010. ISSN 1745-2481. doi: 10.1038/nphys1616.

[10] D. Manzano. A short introduction to the Lindblad master equation. *AIP Advances*, 10(025106), 2020. doi: 10.1063/1.5115323.

[11] Michael A Nielsen and Isaac L Chuang. Quantum Computation and Quantum Information. *Cambridge University Press*, 2010.

[12] A.F. Otte. OtteLab. URL `https://ottelab.tudelft.nl/`.

[13] A. Spinelli, B. Bryant, F. Delgado, J. Fernández-Rossier, and A. F. Otte. Imaging of spin waves in atomically designed nanomagnets. *Nature Materials 2014 13:8*, 13(8):782–785, 7 2014. ISSN 1476-4660. doi: 10.1038/nmat4018. URL `https://www.nature.com/articles/nmat4018`.

[14] R. J. D. Tilley. Understanding Solids: The Science of Materials, 2004.

[15] Lukas M. Veldman, Laëtitia Farinacci, Rasa Rejali, Rik Broekhoven, Jérémie Gobeil, David Coffey, Markus Ternes, and Alexander F. Otte. Free coherent evolution of a coupled atomic spin system initialized by electron scattering. *Science*, 372(6545), 5 2021. ISSN 10959203. doi: 10.1126/SCIENCE.ABG8223/SUPPL{_}FILE/ABG8223-VELDMAN-SM.PDF.

[16] Kai Yang, Yujeong Bae, William Paul, Fabian D. Natterer, Philip Willke, Jose L. Lado, Alejandro Ferrón, Taeyoung Choi, Joaquín Fernández-Rossier, Andreas J. Heinrich, and Christopher P. Lutz. Engineering the Eigenstates of Coupled Spin- 1/2 Atoms on a Surface. *Physical Review Letters*, 119(22), 11 2017. ISSN 10797114. doi: 10.1103/PHYSREVLETT.119.227206.

[17] Kai Yang, William Paul, Soo Hyon Phark, Philip Willke, Yujeong Bae, Taeyoung Choi, Taner Esat, Arzhang Ardavan, Andreas J. Heinrich, and Christopher P. Lutz. Coherent spin manipulation of individual atoms on a surface. *Science (New York, N.Y.)*, 366(6464):509–512, 10 2019. ISSN 1095-9203. doi: 10.1126/SCIENCE.AAY6779.

Chapter A

Appendix

$$\begin{bmatrix} -C_2(0)e^{-\gamma t} + C_4(0) + C_6(0)e^{-2\gamma t} & \left(\frac{-4iJ}{\gamma} + \frac{i\gamma}{4J}\right)C_3(0)e^{(-iJ-1\frac{1}{2}\gamma)t} + C_0(0)e^{-\gamma t} - C_3(0)e^{-2\gamma t} - \frac{1}{4J}i\gamma C_4(0)e^{(iJ-1\frac{1}{2}\gamma)t} \\ \left(\frac{4iJ}{\gamma} - \frac{i\gamma}{4J}\right)C_5(0)e^{(iJ-1\frac{1}{2}\gamma)t} + C_1(0)e^{-\gamma t} - C_5(0)e^{-2\gamma t} + \frac{i\gamma}{4J}C_4(0)e^{(-iJ-1\frac{1}{2}\gamma)t} & -C_2(0)e^{(-iJ-1\frac{1}{2}\gamma)t} - C_3(0)e^{(iJ-1\frac{1}{2}\gamma)t} + C_4(0) - C_6(0)e^{-2\gamma t} \\ \left(-\frac{4iJ}{\gamma} + \frac{i\gamma}{4J}\right)C_5(0)e^{(iJ-1\frac{1}{2}\gamma)t} + C_1(0)e^{-\gamma t} - C_5(0)e^{-2\gamma t} - \frac{i\gamma}{4J}C_4(0)e^{(-iJ-1\frac{1}{2}\gamma)t} & \left(-1 + \frac{i\gamma}{2J}\right)C_2(0)e^{(-iJ-1\frac{1}{2}\gamma)t} + \left(-1 + \frac{i\gamma}{2J}\right)C_3(0)e^{(iJ-1\frac{1}{2}\gamma)t} + C_2(0)e^{-2\gamma t} \\ C_4(0)e^{-2\gamma t} & C_1(0)e^{\gamma t} - C_4(0)e^{(-iJ-1\frac{1}{2}\gamma)t} + C_5(0)e^{(iJ-1\frac{1}{2}\gamma)t} + C_5(0)e^{-2\gamma t} \end{bmatrix}$$

$$\begin{bmatrix} \left(\frac{4iJ}{\gamma} - \frac{i\gamma}{4J}\right)C_3(0)e^{(-iJ-1\frac{1}{2}\gamma)t} + C_0(0)e^{-\gamma t} - C_3(0)e^{-2\gamma t} - \frac{i\gamma}{4J}C_4(0)e^{(iJ-1\frac{1}{2}\gamma)t} & C_1(0)e^{-2\gamma t} \\ \left(-1 - \frac{i\gamma}{2J}\right)C_3(0)e^{(iJ-1\frac{1}{2}\gamma)t} + \left(1 - \frac{i\gamma}{2J}\right)C_2(0)e^{(-iJ-1\frac{1}{2}\gamma)t} + C_2(0)e^{-2\gamma t} & C_0(0)e^{-\gamma t} - C_3(0)e^{(-iJ-1\frac{1}{2}\gamma)t} + C_3(0e^{-2\gamma t} - C_4(0)e^{(iJ-1\frac{1}{2}\gamma)t} \\ C_2(0)e^{(-iJ-1\frac{1}{2}\gamma)t} + C_3(0)e^{(iJ-1\frac{1}{2}\gamma)t} + C_4(0) - C_6(0)e^{-2\gamma t} & C_0(0)e^{-\gamma t} + C_3(0)e^{(-iJ-1\frac{1}{2}\gamma)t} + C_3(0e^{-2\gamma t} + C_4(0)e^{(iJ-1\frac{1}{2}\gamma)t} \\ C_1(0)e^{-\gamma t} + C_4(0)e^{(-iJ-1\frac{1}{2}\gamma)t} + C_5(0)e^{(iJ-1\frac{1}{2}\gamma)t} + C_5(0)e^{-2\gamma t} & C_2(0)e^{-\gamma t} + C_4(0) + C_6(0)e^{-2\gamma t} \end{bmatrix}$$

(A.1)

Comparison between Model 1 and 2 for the Flip-Flop Oscillation

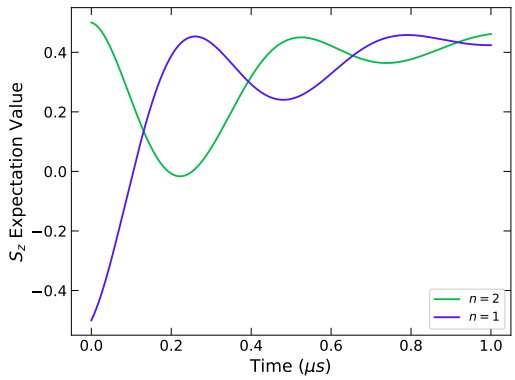

(a) N=2 (Model 2)

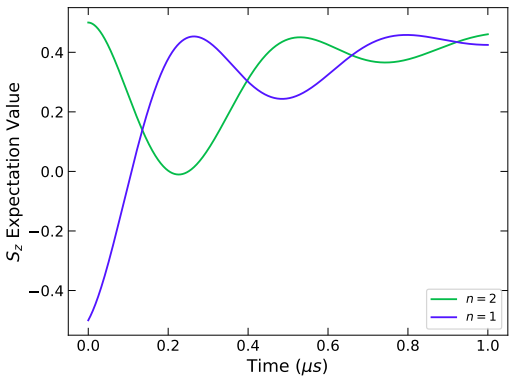

(b) N=2 (Model 1)

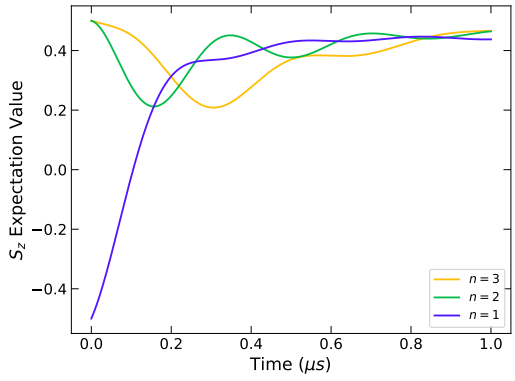

(c) N=3 (Model 2)

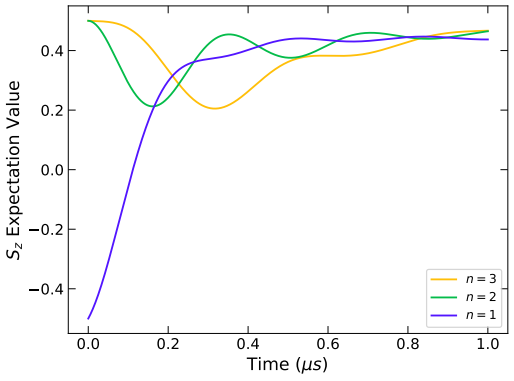

(d) N=3 (Model 1)

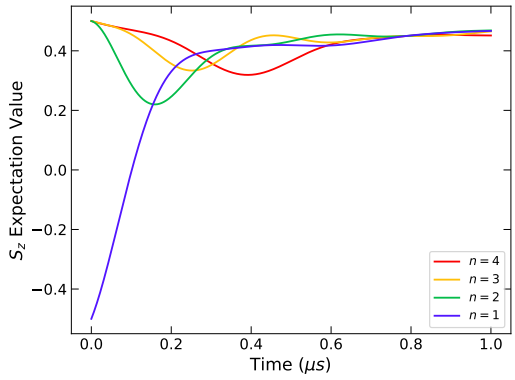

(e) N=4 (Model 2)

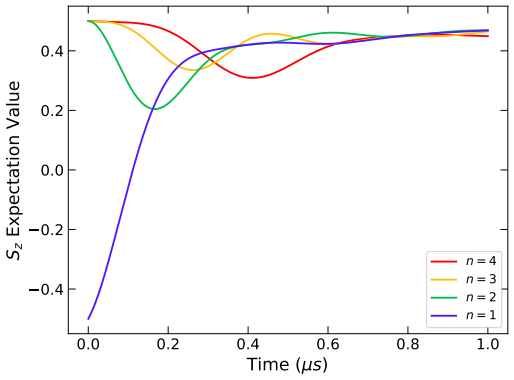

(f) N=4 (Model 1)

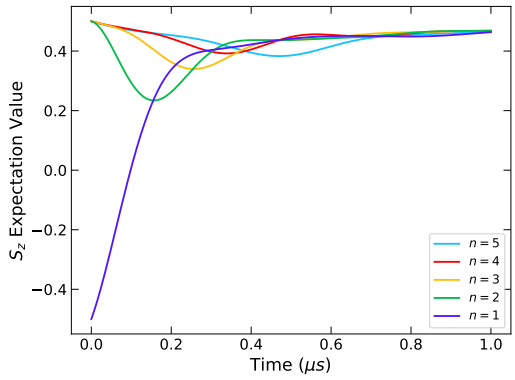

(g) N=5 (Model 2)

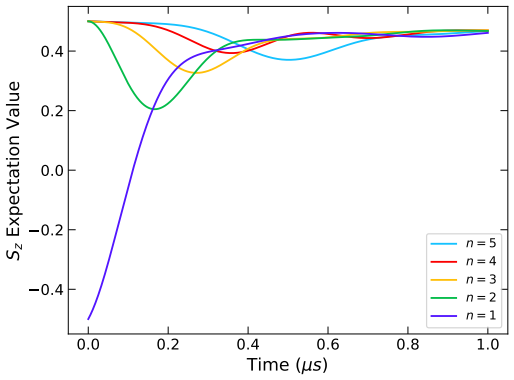

(h) N=5 (Model 1)

Figure A.1: Comparison of Model 1 (Single Particle Decoherence) and Model 2 (Collective Particle Decoherence) for the flip-flop oscillation in S_z expectation value for a range of chain lengths (N=2 to N=5).

Flip-flop Oscillation Coherences

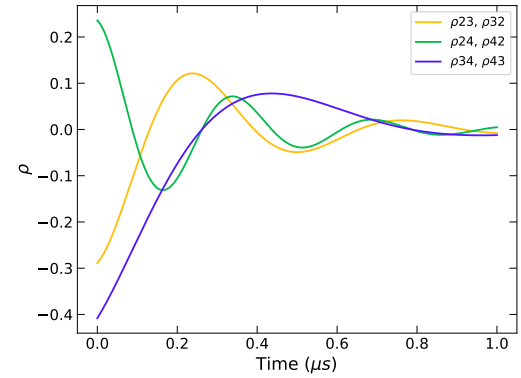

(a) N=3

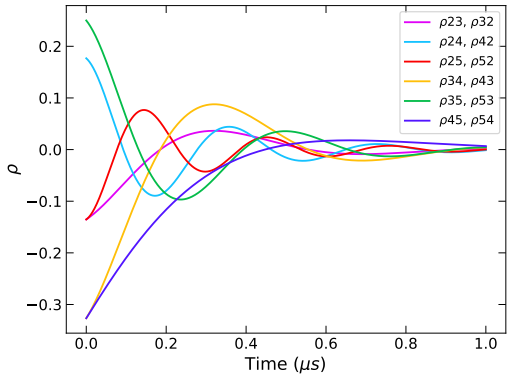

(b) N=4

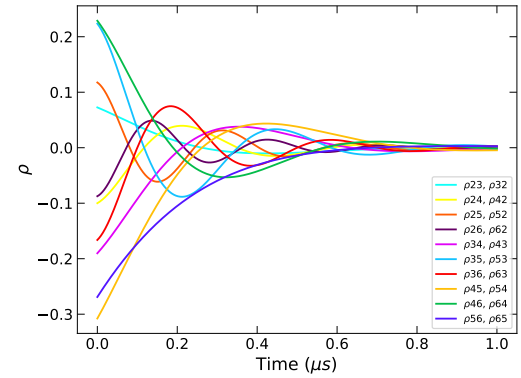

(c) N=5

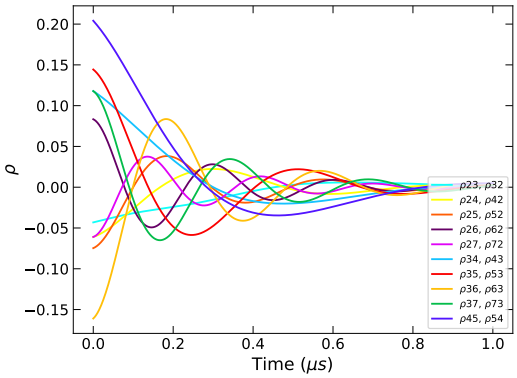

(d) N=6

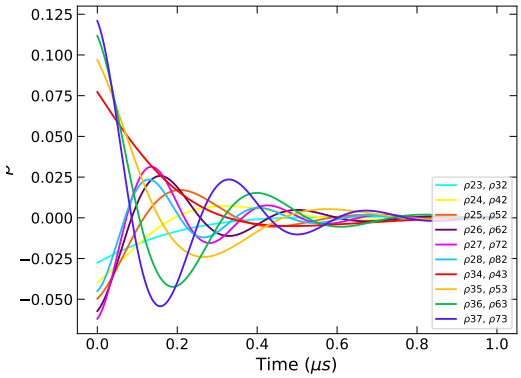

(e) N=7

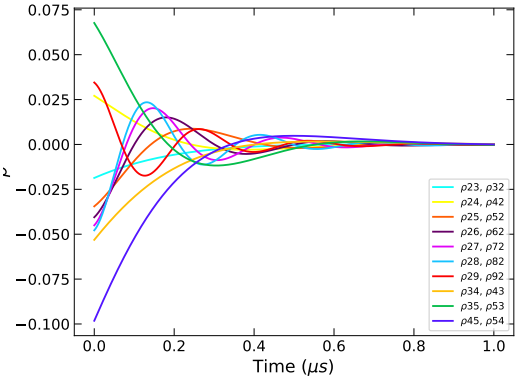

(f) N=8

Figure A.2: Coherences for the flip-flop oscillation in the collective chain decoherence model (model 2) for chain lengths ranging from N=3 to N=8.